

Physics and applications of three-ion ICRF scenarios for fusion research


Cite as: Phys. Plasmas **28**, 020501 (2021); <https://doi.org/10.1063/5.0021818>

Submitted: 24 July 2020 • Accepted: 05 December 2020 • Published Online: 19 February 2021

 Ye. O. Kazakov,  J. Ongena,  J. C. Wright, et al.

COLLECTIONS

Note: The leading four authors received the 2018 Landau-Spitzer Award, jointly granted by APS and EPS.

 This paper was selected as Featured



View Online



Export Citation



CrossMark

ARTICLES YOU MAY BE INTERESTED IN

[Mechanisms of energetic-particle transport in magnetically confined plasmas](#)

Phys. Plasmas **27**, 030901 (2020); <https://doi.org/10.1063/1.5136237>

[Turbulence in space plasmas: Who needs it?](#)

Phys. Plasmas **28**, 032306 (2021); <https://doi.org/10.1063/5.0041540>

[Physics of E×B discharges relevant to plasma propulsion and similar technologies](#)

Phys. Plasmas **27**, 120601 (2020); <https://doi.org/10.1063/5.0010135>

Physics of Plasmas

Papers from 62nd Annual Meeting of the
APS Division of Plasma Physics

Read now!



Physics and applications of three-ion ICRF scenarios for fusion research

Cite as: Phys. Plasmas **28**, 020501 (2021); doi: [10.1063/5.0021818](https://doi.org/10.1063/5.0021818)

Submitted: 24 July 2020 · Accepted: 5 December 2020 ·

Published Online: 19 February 2021



View Online



Export Citation



CrossMark

Ye. O. Kazakov,^{1,a)} J. Ongena,¹ J. C. Wright,² S. J. Wukitch,² V. Bobkov,³ J. Garcia,⁴ V. G. Kiptily,⁵ M. J. Mantsinen,^{6,7} M. Nocente,^{8,9} M. Schneider,¹⁰ H. Weisen,¹¹ Y. Baranov,⁵ M. Baruzzo,¹² R. Bilato,³ A. Chomiczewska,¹³ R. Coelho,¹⁴ T. Craciunescu,¹⁵ K. Crombé,^{1,16} M. Dreval,¹⁷ R. Dumont,⁴ P. Dumortier,^{1,5} F. Durodié,¹ J. Eriksson,¹⁸ M. Fitzgerald,⁵ J. Galdon-Quiroga,³ D. Gallart,⁶ M. Garcia-Muñoz,¹⁹ L. Giacomelli,⁹ C. Giroud,⁵ J. Gonzalez-Martin,¹⁹ A. Hakola,²⁰ P. Jacquet,⁵ T. Johnson,²¹ A. Kappatou,³ D. Keeling,⁵ D. King,⁵ K. K. Kirov,⁵ P. Lamalle,¹⁰ M. Lennholm,⁵ E. Lerche,^{1,5} M. Maslov,⁵ S. Mazzi,^{22,4} S. Menmuir,⁵ I. Monakhov,⁵ F. Nabais,¹⁴ M. F. F. Nave,¹⁴ R. Ochoukov,³ A. R. Polevoi,¹⁰ S. D. Pinches,¹⁰ U. Plank,³ D. Rigamonti,⁹ M. Salewski,²³ P. A. Schneider,³ S. E. Sharapov,⁵ Ž. Štancar,²⁴ A. Thorman,⁵ D. Valcarcel,⁵ D. Van Eester,¹ M. Van Schoor,¹ J. Varje,²⁵ M. Weiland,³ N. Wendler,¹³ JET Contributors,^{b)} ASDEX Upgrade Team,^{c)} EUROfusion MSTI Team,^{d)} and Alcator C-Mod Team

AFFILIATIONS

¹Laboratory for Plasma Physics, LPP-ERM/KMS, TEC Partner, 1000 Brussels, Belgium

²Plasma Science and Fusion Center, Massachusetts Institute of Technology, Cambridge, Massachusetts 02139, USA

³Max-Planck-Institut für Plasmaphysik, 85748 Garching, Germany

⁴CEA, IRFM, 13108 Saint-Paul-Lez-Durance, France

⁵United Kingdom Atomic Energy Authority, Culham Centre for Fusion Energy (CCFE), Culham Science Centre, Abingdon OX14 3DB, United Kingdom

⁶Barcelona Supercomputing Center (BSC), 08034 Barcelona, Spain

⁷ICREA, 08010 Barcelona, Spain

⁸Dipartimento di Fisica, Università di Milano-Bicocca, 20126 Milan, Italy

⁹Institute for Plasma Science and Technology, National Research Council, 20125 Milan, Italy

¹⁰ITER Organization, Route de Vinon-sur-Verdon, CS90046, 13067 St. Paul lez Durance, France

¹¹Swiss Plasma Center, Ecole Polytechnique Fédérale de Lausanne, CH-1015 Lausanne, Switzerland

¹²ENEA for EUROfusion, via E. Fermi 45, 00044 Frascati (Roma), Italy

¹³Institute of Plasma Physics and Laser Microfusion, 01-497 Warsaw, Poland

¹⁴Instituto de Plasmas e Fusão Nuclear, Instituto Superior Técnico, Universidade de Lisboa, 1049-001 Lisboa, Portugal

¹⁵National Institute for Laser, Plasma and Radiation Physics, 077126 Bucharest, Romania

¹⁶Department of Applied Physics, Ghent University, 9000 Gent, Belgium

¹⁷NSC 'Kharkiv Institute of Physics and Technology', 61108 Kharkiv, Ukraine

¹⁸Department of Physics and Astronomy, Uppsala University, SE-75120 Uppsala, Sweden

¹⁹University of Seville, 41013 Seville, Spain

²⁰VTT Technical Research Centre of Finland Ltd., FIN-02044 VTT Espoo, Finland

²¹KTH Royal Institute of Technology, SE-10044 Stockholm, Sweden

²²Aix-Marseille Université, CNRS PIIM, UMR 7345 Marseille, France

²³Department of Physics, Technical University of Denmark, DK-2800 Kgs. Lyngby, Denmark

²⁴Jožef Stefan Institute, SI-1000 Ljubljana, Slovenia

²⁵Aalto University, FIN-00076 Aalto, Finland

Note: The leading four authors received the 2018 Landau-Spitzer Award, jointly granted by APS and EPS.

^{a)}Author to whom correspondence should be addressed: yevgen.kazakov@rma.ac.be

^{b)}See the author list of Joffrin *et al.*, Nucl. Fusion **59**, 112021 (2019).

^{c)}See the author list of Meyer *et al.*, Nucl. Fusion **59**, 112014 (2019).

^{d)}See the author list of Labit *et al.*, Nucl. Fusion **59**, 086020 (2019).

ABSTRACT

This paper summarizes the physical principles behind the novel three-ion scenarios using radio frequency waves in the ion cyclotron range of frequencies (ICRF). We discuss how to transform mode conversion electron heating into a new flexible ICRF technique for ion cyclotron heating and fast-ion generation in multi-ion species plasmas. The theoretical section provides practical recipes for selecting the plasma composition to realize three-ion ICRF scenarios, including two equivalent possibilities for the choice of resonant absorbers that have been identified. The theoretical findings have been convincingly confirmed by the proof-of-principle experiments in mixed H–D plasmas on the Alcator C-Mod and JET tokamaks, using thermal ^3He and fast D ions from neutral beam injection as resonant absorbers. Since 2018, significant progress has been made on the ASDEX Upgrade and JET tokamaks in H– ^4He and H–D plasmas, guided by the ITER needs. Furthermore, the scenario was also successfully applied in JET D– ^3He plasmas as a technique to generate fusion-born alpha particles and study effects of fast ions on plasma confinement under ITER-relevant plasma heating conditions. Tuned for the central deposition of ICRF power in a small region in the plasma core of large devices such as JET, three-ion ICRF scenarios are efficient in generating large populations of passing fast ions and modifying the q -profile. Recent experimental and modeling developments have expanded the use of three-ion scenarios from dedicated ICRF studies to a flexible tool with a broad range of different applications in fusion research.

© 2021 Author(s). All article content, except where otherwise noted, is licensed under a Creative Commons Attribution (CC BY) license (<http://creativecommons.org/licenses/by/4.0/>). <https://doi.org/10.1063/5.0021818>

I. INTRODUCTION

Strong magnetic fields are used to confine plasmas in fusion devices. As a result of the Lorentz force, plasma ions and electrons gyrate around the magnetic field lines with a local characteristic cyclotron frequency $\omega_{cs} = q_s B / m_s$, where q_s and m_s are the charge and the mass of the particle and B is the local value of the magnetic field. Note that ions rotate in the clockwise direction, while electrons rotate counterclockwise, when viewed in the direction opposite to the magnetic field. For typical magnetic fields in present-day and future tokamaks, the ion cyclotron frequencies broadly cover the range between ~ 10 MHz and ~ 100 MHz. A system for plasma heating with waves in the ion cyclotron range of frequencies (ICRF) is under development for ITER, aiming to deliver 20 MW of heating power in the frequency range 40–55 MHz.^{1–4} In addition to plasma heating, ICRF systems have a broad range of additional applications, as discussed in recent overviews.^{5,6}

ICRF heating relies on the excitation of fast magnetosonic waves that can be absorbed by both ions and electrons via a large number of collisionless absorption mechanisms in the plasma.^{7–10} A necessary condition for fundamental ion cyclotron ($n = 1$) and harmonic damping ($n = 2, 3, \dots$) is the local match between the Doppler-shifted wave frequency and the ion cyclotron frequency or harmonics

$$\omega = n\omega_{ci} + k_{\parallel}v_{\parallel,i} \quad (n = 1, 2, 3, \dots). \quad (1)$$

Here, $\omega = 2\pi f$ with f being the frequency of the launched radio frequency (RF) waves; k_{\parallel} and $v_{\parallel,i}$ are the wavenumber and ion velocity parallel to the confining magnetic field; and n is the cyclotron harmonic number. In turn, Eq. (1) determines the parallel velocities for resonant ions

$$v_{\parallel,i} = (\omega - n\omega_{ci}) / k_{\parallel}. \quad (2)$$

For thermal ions with low v_{\parallel} , this condition can be fulfilled close to the ion cyclotron resonance layers, where $\omega \approx n\omega_{ci}$. Note that the physics of ICRF heating is very rich and extends beyond ion cyclotron

interactions only. In particular, fast waves can also be absorbed directly by electrons or undergo a transformation to shorter wavelength modes via mode conversion.^{11,12}

The RF electric field of the propagating fast waves can be written as the sum of a left-hand, E_+ (rotating in the direction of the ions) and a right-hand, E_- (rotating in the direction of the electrons) polarized component.¹³ Efficient ion cyclotron damping for thermal and moderately energetic ions occurs when Eq. (1) is satisfied in a region with a high $|E_+|$.⁹ To a large extent, the plasma composition determines the spatial distribution of the ratio E_+/E_- in the plasma volume and thus is a crucial parameter to optimize the ICRF heating efficiency.

Out of all existing ICRF heating scenarios, minority heating is the most routinely used in fusion research. In its simplest version, this heating scenario is realized in two-ion species plasmas with different charge-to-mass ratios, where the concentration of one of the ion species (minority) is much lower than that of the other one. Minority ions absorb RF power close to their cyclotron resonance, $\omega \approx \omega_{ci, \text{mino}}$ ($n = 1$). In its purest form, minority heating is obtained at a negligible minority concentration that is low enough such that it does not affect the wave propagation characteristics.^{7,8} In practice, minority heating is applied at higher minority concentrations, $X_{\text{mino}} = n_{\text{mino}}/n_e$ (here, n_{mino} is the minority density and n_e is the electron density), typically from a few % to $\sim 10\%$. This is not only due to a higher density of resonant ions, but also because of the appearance of the so-called ion–ion hybrid (IIH) layer.¹⁴ The E_+ component is locally enhanced at this layer (see Sec. II), facilitating RF power absorption by minority ions.

The radial position of the IIH layer in the plasma depends on the plasma composition.¹² As the concentration of minority ions increases, the IIH layer shifts further away from the minority cyclotron resonance toward the cyclotron resonance of the other ion species. Eventually, the distance to the IIH layer gets too large for both plasma ion species and they can no longer resonate at the region with an enhanced $|E_+|$. Under these conditions, ICRF heating via mode conversion becomes dominant, where launched RF fast waves undergo a

transformation into shorter wavelength modes, mostly used (but not only) for local electron heating and plasma flow generation.^{11,12,15,16}

However, there is an elegant solution to transform mode conversion electron heating back into ion cyclotron heating under these conditions. This can be achieved by adding a new degree of freedom to the system and extending the plasma composition beyond two thermal ion species by providing an additional (“third”) ion population.^{17–20} Obviously, a proper choice for the plasma composition is required such that the third resonant ion population satisfies the wave–particle interaction condition, Eq. (1) in the vicinity of a layer with a large $|E_+|$ in such multi-ion species plasmas. In fact, as demonstrated in Sec. II, there are two equivalent possibilities for the choice of the third resonant ion population: (a) an ion population with an intermediate charge-to-mass ratio^{17,18} and (b) a fast-ion population with sufficiently large parallel velocities such that they resonate at the IHH layer because of their large Doppler shift.^{19,20} In the latter case, the charge-to-mass ratio of the resonant absorbers can be the same as for one of the main plasma ions. Thus, in its simplest form, such an ion cyclotron heating scenario can be realized in a plasma composed of at least two ion populations with different charge-to-mass ratios and another population with either a third charge-to-mass ratio or a significantly different parallel velocity; hence, it is called the three-ion ICRF scenario.

In hindsight, this sounds like a trivial idea. In fact, as illustrated in this paper, three-ion scenarios were already effectively at work in D–T, D–³He, and H–D plasmas on TFTR, JET, and ASDEX Upgrade (AUG) (see Sec. IV and references therein). Remarkably, while all the essential elements were recognized by the authors, including the effect of intrinsic and extrinsic impurities on the spatial distribution of $|E_+|$ and ICRF characteristics,^{15,21} the flexibility and tunability of these RF scenarios was apparently not realized as such. These scenarios rely on an active control of the $|E_+|$ RF electric field in the plasma by selecting the plasma mix such that the third ion population resonates in the vicinity of one of the IHH layers. The intentional use of three-ion ICRF scenarios only started a few years ago and highlighted their strong potential and wide range of applications for fusion research beyond plasma heating (see Secs. II, III, and V).

The simplicity of the name should not confuse the reader: nothing prevents applying this ICRF scenario in plasmas with more than three ion populations. In fact, the name of this novel ICRF scenario provides an umbrella for a large variety of options possible in multi-ion species plasmas to transform mode conversion electron heating into a flexible ion cyclotron heating scenario. Note that three-ion ICRF scenarios rely on the fundamental ($n=1$) ion cyclotron damping. As for any other $n=1$ ICRF scenario, the achieved fast-ion energies can be controlled by a number of actuators, including absorbed RF power per resonant ion, plasma density, electron temperature, etc.¹³ This, in turn, allows to control whether collisional electron or bulk ion heating dominates as a result of the slowing-down of the resonant ions.

For a given plasma density, electron heating can be maximized by reducing the number of resonant absorbers and depositing the RF power in the central regions of the plasma. On the other hand, selecting heavier ions and moderating fast-ion energies is beneficial for maximizing collisional bulk ion heating. All this is a consequence of the physics of Coulomb collisions in a plasma, but realizing efficient RF power absorption by heavy ions is not that straightforward. Three-ion ICRF scenarios are particularly suited for this task, as they allow one to

channel RF power to, e.g., ⁹Be impurities in D–T plasmas, with promising applications for ITER and JET with the ITER-like wall (JET-ILW) discussed below.

The examples presented in this paper show that for almost any plasma mix of interest, a suitable three-ion ICRF scenario can be designed for a specific application. The experimental studies carried out so far have shown that these scenarios allow one to probe important aspects of future high-power D–T plasmas. As discussed in the following chapters, the success of the experiments with three-ion ICRF scenarios on the tokamaks Alcator C-Mod, JET, and AUG provided further insights into the plasma effects associated with the presence of MeV-range ions, a field of study that will become more and more important in the near future in fusion research.

Applications of three-ion ICRF scenarios are not only limited to laboratory magnetic confinement plasmas, but also provide further insight into the mechanisms responsible for the acceleration of the ³He ions in ³He-rich solar flares.¹⁸ These events are characterized by an enormous enrichment of the rare isotope ³He (by a factor of $\sim 10^4$) above the solar wind or coronal abundances.^{22,23} Various models have been proposed to explain the anomalous abundance of highly energetic ³He ions. Most of the developed models are based on the ion cyclotron resonance with plasma waves, assumed to be generated by an electron current, energetic electron beams or via coupling with low-frequency Alfvén waves.²³ Our studies show that if proton plasmas additionally include ⁴He ions at the level of $n(^4\text{He})/n_e \approx 10\%–15\%$, the ion cyclotron absorption by a small number of ³He ions can be strongly increased.¹⁸

The paper is organized as follows. In Sec. II, we discuss the theoretical background and provide practical recipes for selecting the plasma composition and resonant absorbers. This is followed by a summary of the main results from proof-of-principle experiments in H–D plasmas in JET and Alcator C-Mod. Section III summarizes recent progress with extended applications of these novel scenarios in H–D, H–⁴He, and D–³He plasmas on AUG and JET. The insights gained over the last few years also provide a common framework to explain puzzling results in some past fast-ion ICRF experiments in D–³He and D–T plasmas in JET and TFTR, discussed in Sec. IV. Section V follows with an overview of promising applications in fusion research, including D–T and nonactive plasmas in ITER. Summary and conclusions are presented in Sec. VI.

II. PROOF-OF-PRINCIPLE EXPERIMENTS IN H–D PLASMAS USING THERMAL ³HE AND FAST D–NBI IONS AS RESONANT ABSORBERS IN THE PLASMA CORE

A. Transforming mode conversion electron heating into a flexible ion cyclotron heating scenario in multi-ion species plasmas: Theoretical background

A basic understanding of fast wave (FW) propagation characteristics in multi-ion species plasmas can be obtained from the cold-plasma dispersion relation, defining the perpendicular FW refractive index (with respect to the confining magnetic field)

$$n_{\perp}^2, \text{FW} \simeq \frac{(\epsilon_L - n_{\parallel}^2)(\epsilon_R - n_{\parallel}^2)}{\epsilon_S - n_{\parallel}^2}. \quad (3)$$

Here, ϵ_S , ϵ_L , and ϵ_R are the plasma dielectric tensor components in the notation of Stix¹³ (involving the contributions of the electrons and all

ion species in the plasma) and $n_{\parallel} = ck_{\parallel}/\omega$ is the parallel refractive index. As discussed in Ref. 9, the ion cyclotron absorption and the fast wave Poynting flux are proportional to $P_{abs} \propto |E_{+}|^2$ and $S_{\perp} \propto n_{\perp} |E_y|^2$, respectively (E_y is the poloidal RF electric field component). Because $|\frac{E_{+}}{E_{-}}| \simeq \left| \frac{\epsilon_R - n_{\parallel}^2}{\epsilon_L - n_{\parallel}^2} \right|$ and $|\frac{E_{+}}{E_y}| \simeq \left| \frac{\epsilon_R - n_{\parallel}^2}{\epsilon_S - n_{\parallel}^2} \right|$, the local damping rate P_{abs}/S_{\perp} is enhanced in regions where the conditions $\epsilon_L = n_{\parallel}^2$ and $\epsilon_S = n_{\parallel}^2$ are satisfied.

A plasma with N ion species with a different charge-to-mass ratios has $N - 1$ successive pairs of ion cyclotron resonances. Between every such pair of cyclotron resonances, there exists a solution for the equation $\epsilon_S(\omega_S) = n_{\parallel}^2$ and $\epsilon_L(\omega_L) = n_{\parallel}^2$, defining the cold-plasma fast wave resonance and the left-hand cutoff, respectively. Throughout the paper, we adopt the notations ‘‘IIH resonance’’²⁴ and ‘‘IIH cutoff’’ for the corresponding FW resonance and left-hand cutoff, and use the term ‘‘IIH layer’’ to loosely refer to the region with the enhanced E_{+} and wave damping around this cutoff-resonance pair. Note that hot-plasma effects impact the FW dispersion, in particular, by bending the FW resonance into a confluence with a kinetic mode. Yet, the cold-plasma approximation is still rather accurate to determine the position of the IIH layers in multi-ion species plasmas.

For example, in two-ion species plasmas and for low k_{\parallel} , the IIH cutoff and resonance frequencies are given by²⁵

$$\omega_L = \frac{\omega_{p1}^2 \omega_{c2}^2 + \omega_{p2}^2 \omega_{c1}^2}{\omega_{p1}^2 \omega_{c2} + \omega_{p2}^2 \omega_{c1}}, \quad \omega_S = \sqrt{\frac{\omega_{p1}^2 \omega_{c2}^2 + \omega_{p2}^2 \omega_{c1}^2}{\omega_{p1}^2 + \omega_{p2}^2}}, \quad (4)$$

where ω_{p1} and ω_{p2} are the plasma frequencies for the two ion species. For these plasmas $Z_1 X_1 + Z_2 X_2 = 1$, and the equation for the IIH cutoff frequency can be simplified further to $\omega_L = Z_1 X_1 \omega_{c2} + Z_2 X_2 \omega_{c1}$. Here, Z_1 and Z_2 are the charge numbers and X_1 and X_2 are the ion concentrations. It is immediately clear that the position of the IIH cutoff can be controlled by varying the plasma composition and that ω_L is located in between ω_{c1} and ω_{c2} . An expression with similar characteristics can be derived for ω_S . For the more general case with N plasma ion species with a different charge-to-mass ratio, the exact plasma composition has to be taken into account to calculate the locations of the $N - 1$ IIH layers (not necessarily all located in the plasma).

At sufficiently large concentrations of the minority ion species, the distance between the IIH layer and the minority cyclotron resonance becomes too large such that minority ions can no longer resonate in the vicinity of the region with enhanced $|E_{+}|$ and electron heating via mode conversion is usually realized.^{12,15} By extending the plasma composition, three-ion ICRF scenarios offer a method to transform local electron heating via mode conversion into an effective technique for ion cyclotron heating in multi-ion species plasmas with a range of applications, as discussed in this paper.

In what follows, we use Z_i and A_i for the charge number and the atomic mass of ion species i , with indices ‘‘1’’ and ‘‘2’’ for the nonresonant main ions such that $(Z/A)_2 < (Z/A)_1$ (i.e., ion species #1 has a larger cyclotron frequency than #2) and index ‘‘3’’ for the resonant absorber population. We also use $X_i = n_i/n_e$ as the notation for the ion concentrations, where n_e is the electron density. As resonant absorbers, a third ion population with a (Z/A) value ‘‘sandwiched’’ between that of the two nonresonant ions, $(Z/A)_2 < (Z/A)_3 < (Z/A)_1$

was proposed in the original theoretical formulation of this ICRF scenario. As discussed in Refs. 17 and 18 and as follows from Eq. (4), efficient ion cyclotron absorption by the third ion population at very small concentrations is maximized at

$$X_1^* \approx \frac{1}{Z_1} \frac{(Z/A)_1 - (Z/A)_3}{(Z/A)_1 - (Z/A)_2}, \quad X_2^* \approx \frac{1}{Z_2} \frac{(Z/A)_3 - (Z/A)_2}{(Z/A)_1 - (Z/A)_2}. \quad (5)$$

In this case, concentrations of resonant absorbers as low as a few % are sufficient to absorb nearly all launched RF power, allowing to maximize the absorbed RF power per resonant ion and, thus, the efficiency of fast-ion generation. This operational space is not readily available for the commonly used minority scenarios, typically being the most effective at minority concentrations of a few %. Note that plasma heating with three-ion ICRF scenarios at larger concentrations of resonant ions is equally possible: in this case, plasma mixtures with $X_1 \gtrsim X_1^*$ and $X_2 \lesssim X_2^*$ are more optimal for fast waves excited from the low magnetic field side (LFS).²⁶

Fast ions with the same (Z/A) as one of the main plasma ions can also be used as resonant absorbers.^{19,20} A natural choice for the realization of the Doppler-shifted version of the three-ion

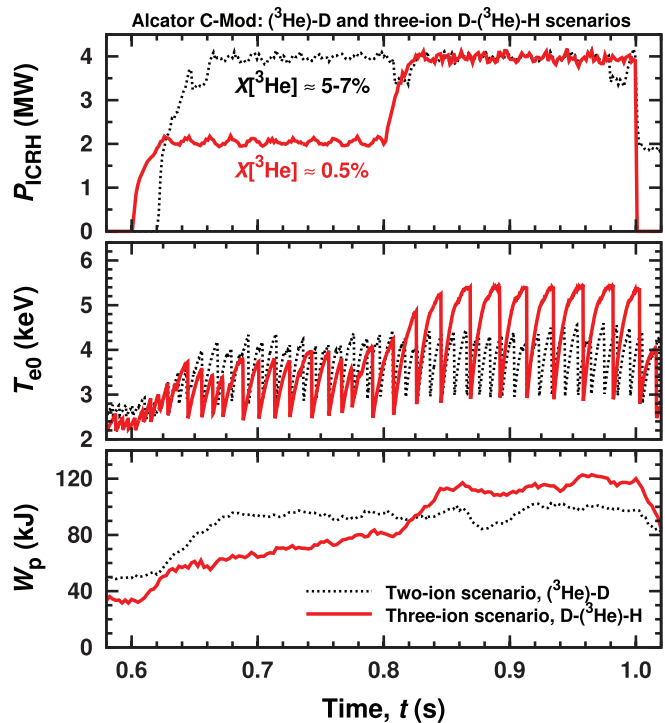


FIG. 1. Proof-of-principle demonstration of the high efficiency of the three-ion ICRF scenario for plasma heating on Alcator C-Mod (7.8 T/1.2 MA, $n_{e0} \approx 2\text{--}3 \times 10^{20} \text{ m}^{-3}$). The panels from top to bottom show the ICRF power, the central electron temperature, and the plasma stored energy. The figure compares the performance of ICRF heating for the three-ion D-(³He)-H scenario (#1160901009, $X[{}^3\text{He}] \approx 0.5\%$, solid lines) and the ³He minority scenario in D plasma (#1160823003, $X[{}^3\text{He}] \approx 5\text{--}7\%$, dotted lines). Reprinted with stylistic modifications with permission of Springer Nature from Kazakov *et al.*, Nat. Phys. 13, 973 (2017). Copyright 2017 EURATOM.

ICRF scenario are fast ions injected by neutral beam injection (NBI). Note that the same physics applies to energetic ions that are products of fusion reactions, as, e.g., fusion-born alpha particles. Absorption of ICRF power by highly energetic alpha particles in D-T plasmas is commonly considered as a parasitic effect to be avoided, but it has a potential to be used to advantage, as discussed in Sec. V D.

For simplicity, we consider plasmas where the resonant fast ions have the same charge-to-mass ratio as ion species #2 according to the adopted definitions, i.e., $(Z/A)_2 < (Z/A)_1$. In this case, the IIH layer is located in the low magnetic field side direction with respect to the cyclotron resonance of ion species #2. This implies that fast ions with a positive Doppler shift ($k_{\parallel v_{\parallel}} > 0$) are required to resonate at this layer. Efficient RF power absorption by fast ions is realized in plasmas with a composition given by $X_1 \approx X_1^*$ and $X_2 \approx X_2^*$, where

$$\begin{aligned} X_1^* &\approx \frac{1}{Z_1} \frac{(Z/A)_1 - (Z/A)_2 / (1-p)}{(Z/A)_1 - (Z/A)_2}, \\ X_2^* &\approx \frac{1}{Z_2} \frac{(Z/A)_2}{(Z/A)_1 - (Z/A)_2} \frac{p}{1-p}. \end{aligned} \quad (6)$$

Here, $p = \delta R_{\text{fast}}^{(\text{max})} / R_{\text{abs}}$, R_{abs} is the intended radial location for RF power absorption (for core heating $R_{\text{abs}} \approx R_0$), $\delta R_{\text{fast}}^{(\text{max})} = \frac{B_{\text{tor}}}{B} \frac{n_{\text{tor}}^{(\text{max})}}{\omega}$ is the Doppler-shift distance for fast ions with maximum parallel velocities, and n_{tor} is the fast wave toroidal mode number, $k_{\parallel} \approx (B_{\text{tor}}/B) (n_{\text{tor}}/R)$. The factor B_{tor}/B in these expressions ensures the proper sign for k_{\parallel} and δR_{fast} along the magnetic field, regardless the choice for the orientation of the toroidal angle. Using the formal substitution

$$(Z/A)_3 \leftrightarrow (Z/A)_2 / (1-p), \quad (7)$$

one easily finds the equivalence of Eqs. (5) and (6). This equivalence further highlights the main idea behind three-ion ICRF scenarios: extending the plasma composition beyond two ion species to include an additional population of ions capable to satisfy the resonance condition, Eq. (1) at the location of the IIH layer.

One can easily derive similar formulas when the resonant fast ions have the same charge-to-mass ratio as ion species #1, i.e., those with $(Z/A)_1 > (Z/A)_2$. Then, the IIH layer is located toward the high magnetic field side (HFS) direction with respect to the cyclotron resonance of ion species #1 and fast ions with a negative Doppler shift ($k_{\parallel v_{\parallel}} < 0$) are required to resonate at this layer.

We also introduce the following notation for three-ion ICRF scenarios: Y_2 –(Y_3)– Y_1 , where the resonant absorbers Y_3 are indicated between the round brackets, and Y_2 and Y_1 are the nonresonant ions ordered according to their (Z/A) value ($\omega_{c2} < \omega_{c1}$). For example, the notations D–(^3He)–H and D–(D_{NBI})–H stand for three-ion ICRF scenarios in mixed H–D plasmas, using ^3He and D–NBI ions as resonant absorbers, respectively.

B. Proof-of-principle experiments with resonant ^3He ions in mixed H–D plasmas on Alcator C-Mod and JET

Mixed H–D plasmas with ^3He ions as resonant absorbers (with their unique $(Z/A) = 2/3$) were chosen for the proof-of-principle

demonstration of these novel ICRF scenarios on the Alcator C-Mod and JET tokamaks. As reported in Ref. 18, the experimental studies on Alcator C-Mod were performed at a very high toroidal magnetic field $B_0 = 7.8$ T, plasma current $I_p = 1.2$ MA and high central electron densities $n_{e0} \approx 2\text{--}3 \times 10^{20} \text{ m}^{-3}$. 4–5 MW of ICRF power was delivered into this plasma at RF frequencies $f = 78.0\text{--}80.0$ MHz for the core ^3He heating. Figure 1 shows the time evolution of the ICRF power, central electron temperature T_{e0} , and plasma stored energy W_p for a pulse with the ^3He minority scenario in a D plasma ($X[^3\text{He}] \approx 5\%\text{--}7\%$, black dotted lines), and a pulse with the three-ion D–(^3He)–H scenario in a H–D plasma ($X[^3\text{He}] \approx 0.5\%$, red solid lines). The high efficiency of the three-ion ICRF scenario for plasma heating is clearly seen by comparing the time traces for T_{e0} and the plasma stored energy at the same RF power, $P_{\text{ICRF}} = 4$ MW. The novel ICRF scenario was also effective in generating highly energetic ^3He ions in the plasma, as testified by an increased sawtooth period (the presence of fast ions is well known to have a stabilizing effect on sawteeth²⁷) and the excitation of Alfvén eigenmodes (AEs).¹⁸

The high efficiency of this novel ICRF scenario was independently confirmed on the world-largest tokamak currently in operation, JET ($R_0 \approx 3$ m, $a \approx 1$ m). Due to its larger size and higher plasma current, multi-MeV ^3He ions are well confined in JET and, thus, effective plasma heating was achieved at even lower ^3He concentrations than in Alcator C-Mod. Figure 2(a) shows an overview of JET pulse #90758 (3.2 T/2 MA, $n_{e0} \approx 4 \times 10^{19} \text{ m}^{-3}$, $f = 32.2\text{--}33.0$ MHz), where $n(^3\text{He})/n_e \approx 0.2\%$ was successfully controlled by the ^3He real-time control system (RTC), measuring its concentration at the plasma edge.^{12,28} Multi-MeV range ^3He ions were generated in those experiments, as confirmed by a suite of fast-ion diagnostics at JET, including gamma-ray spectroscopy.²⁹ Similar to Alcator C-Mod results, long-period sawteeth and ^3He -driven tornado toroidicity-induced AE (TAE) modes³⁰ were observed in JET experiments.

Figure 2(b) illustrates that the three-ion ICRF scenario is also efficient for plasma heating at higher ^3He concentrations (#90756). At the start of this pulse, the ^3He concentration was kept at a very low level $\sim 0.2\%$ by the ^3He RTC system. The measured T_e and T_i profiles highlight that not only electrons, but also bulk ions were effectively heated [not shown here; see Fig. 3(b) in Ref. 31]. As the concentration of ^3He ions was gradually increased to $\sim 1.5\%$, efficient plasma heating continued to be observed, demonstrating the robustness of the heating scenario to variations in $n(^3\text{He})/n_e$ within this range and to inherent uncertainties with measuring the ^3He concentration in the core regions of the plasma. Although JET has a limited experience with the application of this scenario at ^3He minority concentrations of $\sim 1\%$, these first results are encouraging.

JET also demonstrated effective plasma heating with this novel scenario, when NBI was not available and the plasma was heated by ICRF only. A clear illustration is shown in Ref. 32, where JET pulse #91304 (3.1 T/1.8 MA, $P_{\text{ICRF}} \approx 4.4$ MW, $+\pi/2$ phasing) and the corresponding fast-ion observations are discussed in detail. In that pulse, not only tornado TAEs, but also ellipticity-induced AE (EAEs) were excited by multi-MeV ^3He ions generated with the three-ion ICRF scenario.

C. Proof-of-principle experiments with resonant fast D–NBI ions in mixed H–D plasmas on JET

In the summer of 2016, we also designed and conducted dedicated experiments in mixed H–D plasmas in JET to demonstrate the

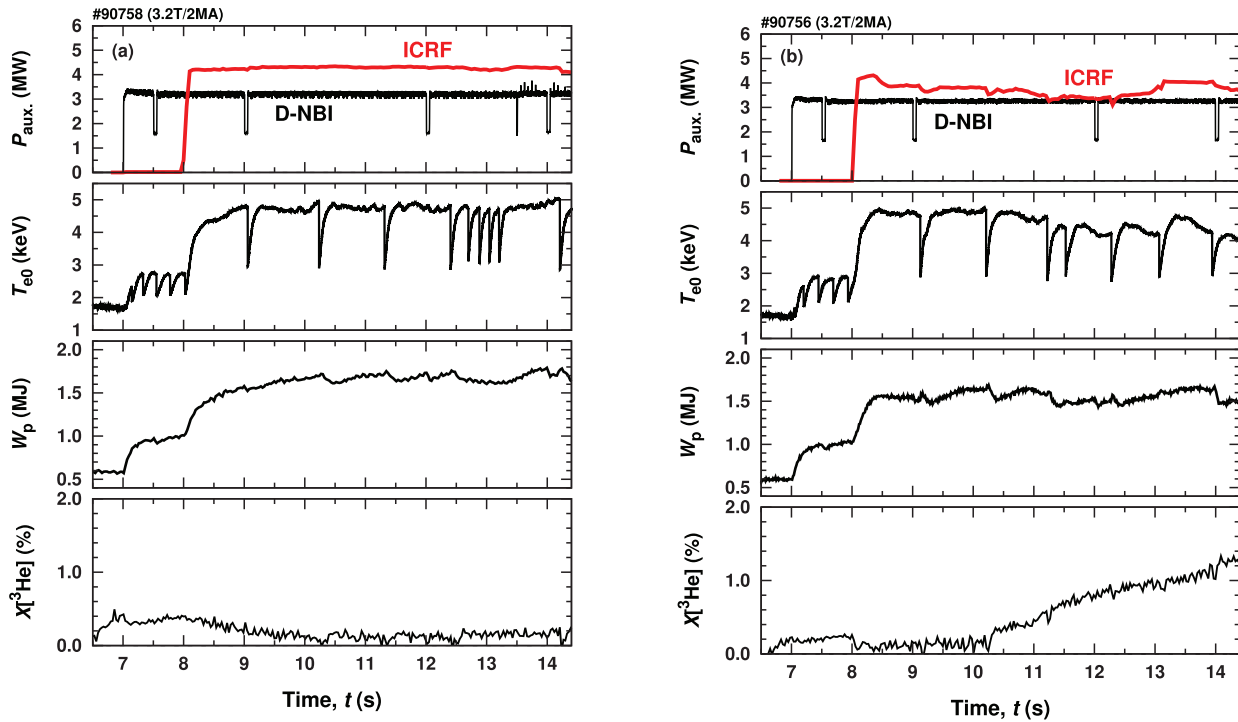


FIG. 2. Overview of JET pulses #90758 (a) and #90756 (b), in which the three-ion D-(³He)-H scenario was applied to generate fast ³He ions and for plasma heating (3.2 T/2 MA, $n_{e0} \approx 4 \times 10^{19} \text{ m}^{-3}$, $f = 32.2\text{--}33.0 \text{ MHz}$, and $+\pi/2$ ICRF antenna phasing). As seen from the figure, efficient heating of the background mixed H-D plasma was observed both at very low ³He minority concentrations, $n(^3\text{He})/n_e \approx 0.2\%$ and at higher ³He concentrations, up to $\sim 1.5\%$.

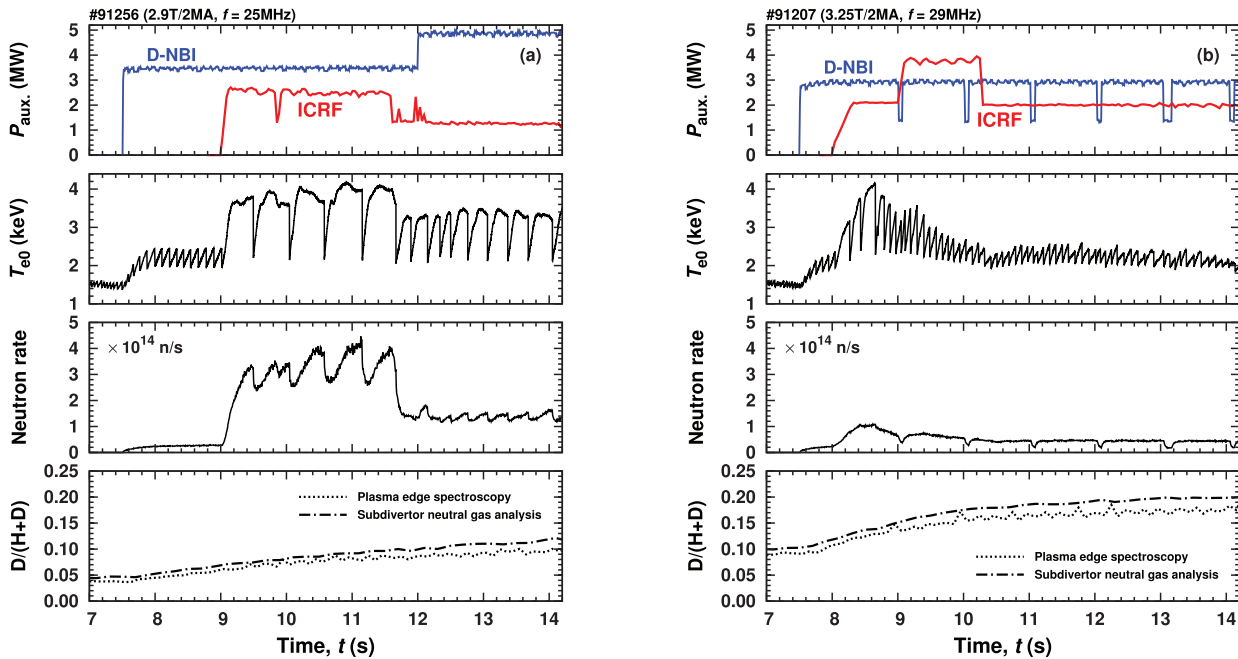


FIG. 3. (a) Overview of JET pulse #91256 (2.9 T/2 MA, $n_{e0} \approx 4 \times 10^{19} \text{ m}^{-3}$, $f = 25.0\text{--}25.6 \text{ MHz}$, dipole phasing), in which the three-ion D-(D_{NBI})-H scenario was successfully applied for plasma heating and generation of energetic D ions in the core of mixed H-D plasmas. (b) Overview of JET pulse #91207 (3.25 T/2 MA, $f = 29 \text{ MHz}$, dipole phasing), in which the three-ion scenario was attempted, but not successful. Similar to the conditions for pulse #91256, the Doppler-shifted resonance for fast D-NBI ions was located in the plasma core, but there was a mismatch with the position of the ICH layer because of the higher D/(H + D).

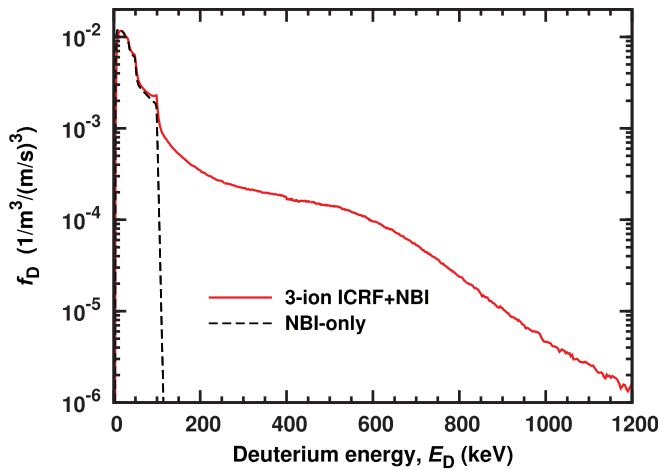


FIG. 4. The computed TRANSP/TORIC distribution function of fast D ions for the conditions of JET pulse #91256: NBI-only heating (dashed line) vs three-ion D-(D_{NBI})-H ICRF + NBI scenario (solid line).

efficiency of the three-ion D-(D_{NBI})-H ICRF + NBI scenario.^{19,20} In this case, the radial location of the IHH layer is actively controlled by properly selecting the concentrations of the H and D ions, while the role of NBI system is to provide resonant absorbers at the IHH layer. Thus, the (Z/A) value of the resonant NBI ions can be the same as for the main plasma ions. In these proof-of-principle JET experiments, a combination of D-NBI ($E_{\text{NBI}} \approx 100$ keV, tangential injectors with pitch $\lambda = v_{\parallel}/v \approx 0.62$), and ICRF heating ($f = 25.0$ – 25.6 MHz, dipole phasing) was applied. Figure 3(a) shows an overview of JET pulse #91256 (2.9 T/2 MA, $n_{e0} \approx 4 \times 10^{19} \text{ m}^{-3}$ controlled by the gas fueling feedback system), which is an illustrative example of what can be achieved. Following our theoretical calculations, see Eq. (6), the plasma composition ($X[\text{H}] \approx 85\%$ – 90% , $X[\text{D}] \approx 10\%$ – 15%) and operational settings were purposely chosen to locate the cyclotron resonance of thermal D ions HFS off-axis, while positioning the IHH layer in the plasma core. As shown in Fig. 3(a), a strong increase in T_{e0} and neutron rate was achieved in the combined ICRF + NBI phases. In this pulse, the maximum neutron rate (enhanced by a factor of ~ 10 – 15 with respect to the phase with NBI-only) was achieved in the phase with $P_{\text{NBI}} \approx 3.5$ MW and $P_{\text{ICRF}} \approx 2.5$ MW, when the isotopic ratio $\text{D}/(\text{H} + \text{D})$ was ~ 0.10 .

This pulse has been extensively modeled with the PION³³ and TRANSP/TORIC codes,^{34,35} which compute the time-evolution of ICRF power absorption and the distribution functions of the resonant ions, as reported in Refs. 36 and 37. The observed neutron rate enhancement cannot be explained by the increase in T_e alone. Indeed, the simulations show an increase in the neutron rate by a factor of ~ 1.5 – 2 only, when the increase in plasma temperature is included in the simulations, but the ICRF + NBI synergies are excluded. Figure 4 shows the distribution function of fast D ions in the core of JET plasmas in the phase of pulse #91256 with 3.5 MW of NBI and 2.5 MW of ICRF, computed by TRANSP/TORIC including the ICRF + NBI synergies. The figure clearly illustrates the formation of high-energy D ions with energies up to ~ 1.5 MeV, well above the NBI injection energy ($E_{\text{NBI}} = 100$ keV). The computed TRANSP/TORIC

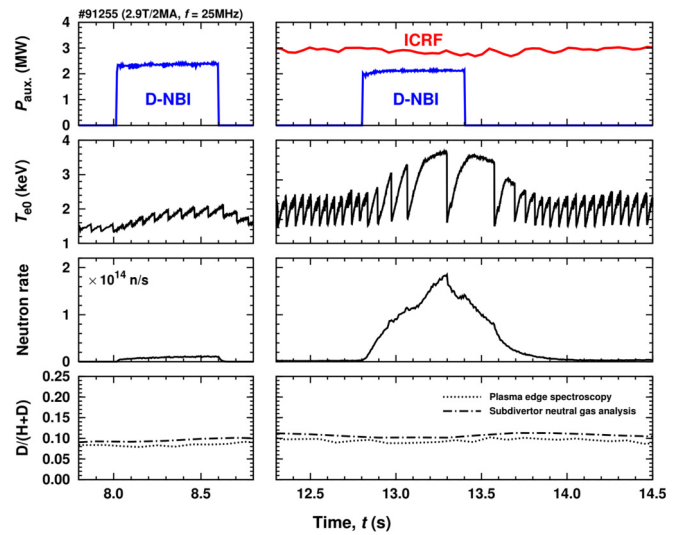


FIG. 5. Didactic illustration of the principle behind three-ion ICRF + NBI scenarios. In JET pulse #91255, high-energy D ions were effectively generated, when the NBI system provided resonant absorbers at the IHH layer, as seen from the time traces for the neutron rate and T_{e0} . When the resonant absorbers were not supplied by the NBI, the three-ion D-(D_{NBI})-H ICRF scenario was converted back to electron heating via mode conversion in the H-D plasma. For comparison, the left panel shows the phase with D-NBI heating only in the beginning of the discharge.

distribution function of energetic D ions was validated against a range of JET fast-ion diagnostics, including the total neutron rate, the time-of-flight neutron spectrometer TOFOR, the spatial neutron emission profile, and the neutral particle analyzer (NPA) measurements.³⁷

In fact, pulse #91256 had two combined ICRF + NBI phases with the same total auxiliary heating power ($P_{\text{aux}} \approx 6.0$ – 6.2 MW), but different ratio $P_{\text{ICRF}}/P_{\text{NBI}} \approx 0.7$ and 0.3 . Substantially lower neutron rates were obtained in the phase at lower ICRF power. PION modeling managed to reproduce the complex evolution of the neutron rate during the pulse at different NBI and ICRF powers.³⁶ In particular, the PION simulations highlighted that the ratio $P_{\text{ICRF}}/P_{\text{NBI}}$ (at the total auxiliary heating power) is a strong actuator to control the fast-ion distributions generated by three-ion ICRF + NBI scenarios. The possibility to tailor the fast-ion energy distributions from moderately high (\sim a few hundred keV) to very high (~ 1 MeV and higher) is one of the advantages of these novel scenarios. This feature is particularly relevant for studies in D-³He and D-T plasmas by maximizing fast-ion populations at moderate energies where the corresponding fusion reactivities have a maximum.¹⁹

For comparison, we also show the performance of JET pulse #91207 (3.25 T/2 MA, $f = 29$ MHz) with the same radial arrangements for the ion cyclotron resonances as in pulse #91256. In both pulses, the cyclotron resonance of thermal D ions was located HFS off-axis [$\omega_{\text{CD}}(0)/\omega \approx 0.85$ – 0.88] and the Doppler-shifted resonance of fast D-NBI ions was in the plasma core. Nevertheless, the results of JET pulse #91207 were quite disappointing—much lower T_{e0} and neutron rate—as seen in Fig. 3(b). In this pulse, the synergetic effects are only visible at the very beginning of the combined ICRF + NBI phase when $\text{D}/(\text{H} + \text{D}) \approx 0.11$ – 0.14 . The neutron rate and T_{e0} very quickly drop with increasing $\text{D}/(\text{H} + \text{D}) \approx 0.15$ – 0.20 as a consequence of a

further radial shift of the IIH layer. Under these conditions, the NBI system did not provide resonant absorbers at the position of the IIH layer.

Another illustration of the importance to satisfy both conditions simultaneously is demonstrated in Fig. 5. In pulse #91255 (2.9 T/2 MA, $f = 25.0\text{--}25.6$ MHz, dipole phasing), the isotopic ratio was nearly constant $D/(H+D) \approx 0.10$ such that the radial position of the IIH layer remained fixed in the plasma during the pulse. The pulse was first heated with D-NBI only ($t = 8.0\text{--}8.6$ s), leading to a relatively small increase in the neutron rate, as shown on the left panel of Fig. 5. In a later phase of the pulse, the plasma was heated with ~ 3 MW of ICRF power only, showing an even lower neutron rate as compared to the NBI-only phase. Only when ICRF and NBI were applied simultaneously, high-energy D ions were effectively generated, leading to a strong increase in the neutron rate, T_{e0} and sawtooth stabilization. When NBI was again switched off at $t = 13.4$ s, the three-ion D-(D_{NBI})-H ICRF scenario lacked resonant absorbers at the IIH layer and, as a result, electron heating via mode conversion in a H-D plasma was recovered. In short, the following sequence of ICRF heating scenarios was realized in JET pulse #91255: mode conversion \rightarrow ion cyclotron heating of D-NBI ions with the three-ion D-(D_{NBI})-H scenario \rightarrow mode conversion. This example highlights how by cleverly combining several effects that are individually well-known, one can realize a new very efficient ICRF scenario for ion cyclotron heating and fast-ion generation in mixed plasmas.

III. RECENT PROGRESS WITH APPLICATIONS OF THREE-ION ICRF SCENARIOS

In this section, we present an overview of new experimental results obtained after receiving the Landau-Spitzer Award in 2018. Significant progress has been obtained since then on JET and AUG, expanding the use of the scenarios from ICRF-dedicated studies to a flexible tool with a broad range of different applications in fusion research. Much of these recent developments were guided by the updated ITER Research Plan within the Staged Approach (2018).³⁸ This document reflects the ITER strategy for physics and technology research for both the Pre-Fusion Power Operation (PFPO) and the Fusion Power Operation (FPO) phases. Various three-ion ICRF scenarios were explicitly included in the document as they hold promises for both PFPO and the FPO phases of ITER.

As shown in this section, three-ion ICRF scenarios have become an important tool for the following physics topics:

- Generation of fusion-born alpha particles in D-³He plasmas in view of the validation of JET-ILW diagnostics for alpha particle measurements in preparation for future D-T studies.
- Investigation of fast-ion driven MHD instabilities on plasma confinement.
- Contribute to a further understanding of the impact of fast ions on microturbulence under ITER-relevant conditions with dominant fast-ion electron heating.
- Development of an off-axis heating scenario for L- to H-mode transition studies in H-D and H-⁴He plasmas, in view of widening the H-mode operational space in the PFPO phase of ITER.

A. Demonstration of the D-(D_{NBI})-³He scenario in D-³He plasmas on JET

Following the success with the three-ion ICRF scenario to accelerate D-NBI ions in mixed H-D plasmas (see Sec. II C), the effectiveness of accelerating D-NBI ions was also demonstrated in D-³He plasmas on JET.^{20,39} The experimental conditions ($B_0 \approx 3.7$ T, $I_p = 2.5$ MA, $n_{e0} \approx 6 \times 10^{19} \text{ m}^{-3}$, $f = 32.2\text{--}33.0$ MHz, dipole phasing) were chosen such that the cyclotron resonances for thermal D and ³He ions were located at the HFS and LFS off-axis, respectively (see Fig. 6). In these experiments, large concentrations of ³He ions were used, $n(^3\text{He})/n_e \approx 20\%\text{--}25\%$ to purposely position the IIH layer in the plasma core. Similar to pulse #91256, tangential NBI injectors with $E_{\text{NBI}} \approx 100$ keV were used to provide resonant absorbers at the IIH layer to absorb locally RF power. In this way, deuterons from the NBI system were accelerated to higher energies with ICRF in the plasma core, which leads to the generation of alpha particles from D-³He fusion reactions



In a similar way, alphas were produced in earlier fast-ion experiments on JET with third harmonic ICRF acceleration of D-NBI ions in D-³He plasmas.⁴⁰ While in both fast-ion experiments ³He ions were the target for the $D + {}^3\text{He}$ fusion reactions, in the experiments

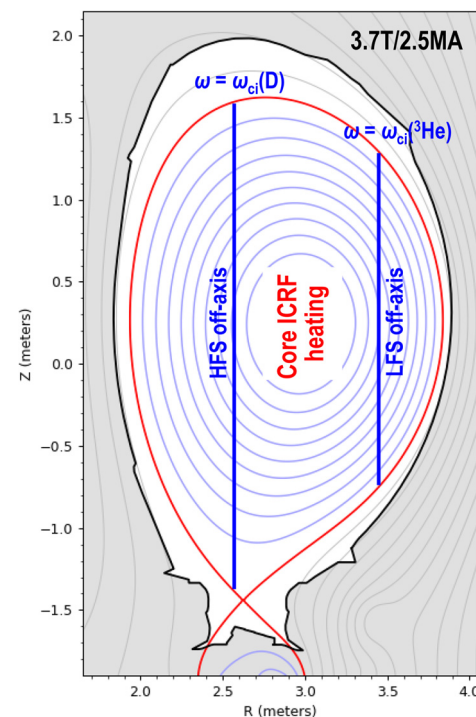


FIG. 6. The poloidal cross section of the JET tokamak with the off-axis location of the ion cyclotron resonances for thermal D and ³He ions for three-ion ICRF experiments in D-³He plasmas (3.7 T/2.5 MA, $n_{e0} \approx 6 \times 10^{19} \text{ m}^{-3}$, $f = 32.2\text{--}33.0$ MHz, dipole phasing, $E_{\text{NBI}} \approx 100$ keV).

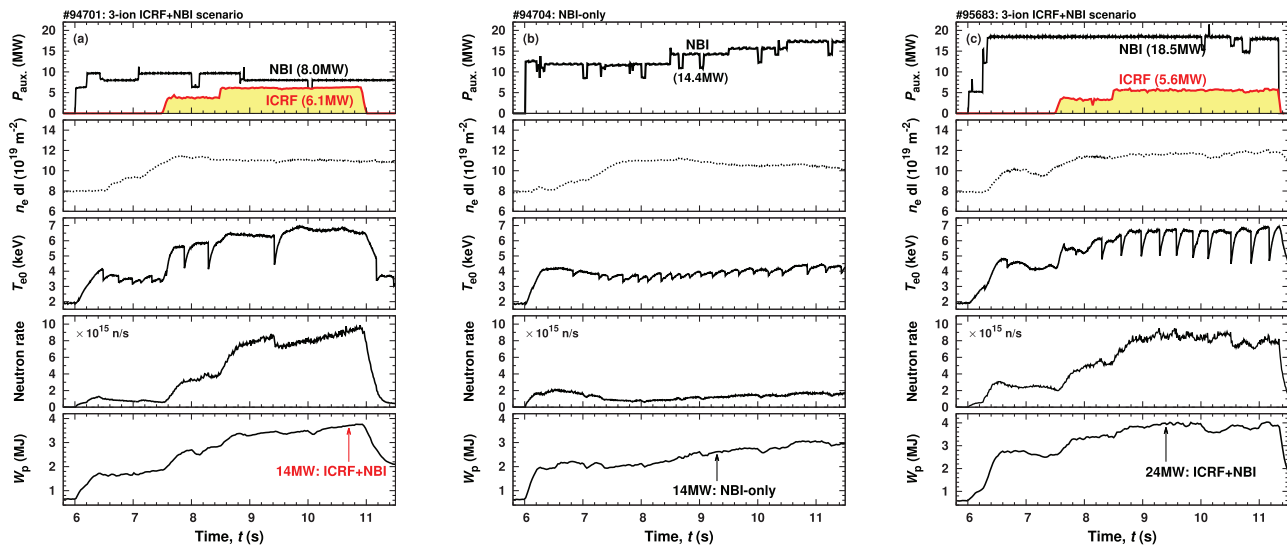


FIG. 7. Overview of JET pulses in mixed $D\text{-}^3\text{He}$ plasmas ($3.7\text{ T}/2.5\text{ MA}$, $n_{e0} \approx 6 \times 10^{19}\text{ m}^{-3}$, $n(^3\text{He})/n_e \approx 20\% \text{--} 25\%$): (a) #94701, (b) #94704, and (c) #95683. In pulse #94704, NBI-only heating was applied in steps from 11.8 MW to 17.3 MW . In pulses #94701 and #95683, the three-ion $D\text{-}(D_{\text{NBI}})\text{-}^3\text{He}$ scenario was applied with $P_{\text{ICRF}} \approx 6\text{ MW}$ (dipole phasing) and $P_{\text{NBI}} \approx 8\text{ MW}$ and $P_{\text{NBI}} \approx 18.5\text{ MW}$, respectively.

described here, the ^3He ions also played an active role for ICRF heating by defining the radial position of the IIH layer and thus the localization of the source of fast ions.

Guided by PION modeling results,³⁶ the fast-ion distribution of RF-accelerated $D\text{-NBI}$ ions in these experiments was controlled by varying the ICRF and NBI power and their ratio $P_{\text{ICRF}}/P_{\text{NBI}}$ ($P_{\text{ICRF}} \approx 4\text{--}6\text{ MW}$, $P_{\text{NBI}} \approx 3\text{--}20\text{ MW}$). With as little as $P_{\text{RF}} \approx 6\text{ MW}$ and $P_{\text{NBI}} \approx 7\text{--}11\text{ MW}$, rather high $D\text{-D}$ neutron ($\sim 1 \times 10^{16}\text{ s}^{-1}$) and $D\text{-}^3\text{He}$ alpha rates ($\sim 2 \times 10^{16}\text{ s}^{-1}$) were achieved, corresponding together to $\sim 60\text{--}70\text{ kW}$ of fusion power.

Figure 7(a) gives an overview of JET pulse #94701, in which $\sim 8\text{ MW}$ of NBI was applied in combination with ICRF in steps from $\sim 4\text{ MW}$ to $\sim 6\text{ MW}$. The panels from top to bottom illustrate P_{NBI} and P_{ICRF} , the line-integrated central density, the central electron temperature, the neutron rate, and the plasma stored energy. The neutron rate increased from $\sim 7 \times 10^{14}\text{ s}^{-1}$ in the NBI-only phase to $\sim 3.7 \times 10^{15}\text{ s}^{-1}$ in the first ICRF + NBI phase with 4 MW of ICRF. Topping up ICRF power with 2 MW from the ITER-like antenna (ILA), monster sawteeth appeared, accompanied by a gradual increase in the neutron rate up to $\sim 9.4 \times 10^{15}\text{ s}^{-1}$. Such a strong enhancement of the neutron rate in the ICRF + NBI phase results from the presence of a large population of energetic D ions, further evidenced by the neutron spectrometer and NPA measurements.

We also show an overview of two other JET pulses in $D\text{-}^3\text{He}$ plasmas at similar operational conditions, but different NBI and ICRF power. Figure 7(b) illustrates pulse #94704, in which NBI-only heating was applied in steps from $\sim 11.8\text{ MW}$ to $\sim 17.3\text{ MW}$. Figure 7(c) shows the time traces for pulse #95683, in which the three-ion $D\text{-}(D_{\text{NBI}})\text{-}^3\text{He}$ scenario was applied, but at much higher NBI power, $P_{\text{NBI}} \approx 18.5\text{ MW}$.

We first start the comparison between pulses #94701 and #94704 at the same total auxiliary heating power $P_{\text{aux}} \approx 14\text{ MW}$. The main difference between the two pulses is the heating source. Dominant ion heating was provided with NBI-only in pulse #94704. Conversely,

dominant electron heating was obtained in pulse #94701 by accelerating fast ions to energies well above the critical energy ($E_{\text{crit}} \approx 300\text{ keV}$) using the three-ion ICRF scenario ($P_{\text{NBI}} \approx 8\text{ MW}$, $P_{\text{ICRF}} \approx 6\text{ MW}$). Among others, this is evidenced by the neutron

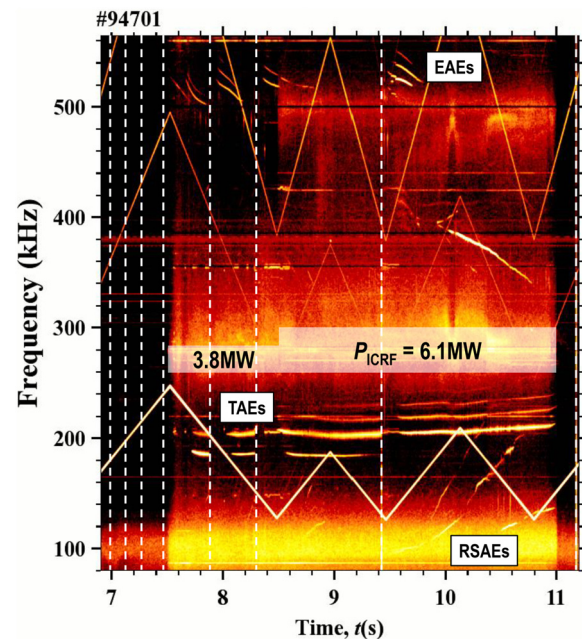


FIG. 8. A large variety of fast-ion driven AEs are regularly observed at JET, when applying three-ion ICRF scenarios to maximize core plasma heating and fast-ion generation. As an example, we show the MHD spectrogram for JET pulse #94701, in which the three-ion $D\text{-}(D_{\text{NBI}})\text{-}^3\text{He}$ scenario was applied and reversed-shear Alfvén eigenmodes (RSAEs), TAEs, and EAEs were observed. The vertical dashed lines indicate the timing of the sawtooth crashes.

time-of-flight spectrometer TOFOR, showing the presence of D ions with tail energies up to $\sim 2\text{--}2.5$ MeV.⁴¹ Furthermore, a rich variety of Alfvénic eigenmodes (AEs) was driven by the energetic ions in #94701, see Fig. 8. In contrast, no fast-ion driven AEs were observed in #94704.

The comparison of the radial T_e and T_i profiles for these two pulses is shown in Fig. 9. The electron temperature profile was measured by the electron cyclotron emission diagnostic and the ion temperature profile by charge exchange recombination spectroscopy (CXRS) based on neon impurities, which were injected on purpose for T_i measurements. The stronger T_e peaking, the much higher T_{e0} and neutron rate in pulse #94701, as compared to #94704, are easily understood by the presence of high-energy D ions. Interestingly, very similar ion temperatures were reached in these two pulses, despite the substantial difference in the ion/electron heating sources. The comparison of the measured T_e and T_i profiles and the plasma stored energy [cf. Figs. 7(a) and 7(b)] hints at better plasma confinement in pulse #94701. Characterized by a large fraction of energetic ions in the plasma core, the heating conditions in #94701 approach those expected in burning plasmas of ITER with alpha particles. Despite dominant fast-ion electron heating in #94701, $T_i \approx T_e$ was observed, which is very promising in view of ITER. This experimental observation is supported by the detailed gyrokinetic analysis of #94701 with the GENE code,⁴² showing that the ion-temperature-gradient (ITG) driven turbulence was suppressed in the presence of MeV ions and fully destabilized TAEs, see Ref. 41. The application of three-ion ICRF scenarios as a tool for turbulence studies, in particular, to study the complex interplay between microturbulence, fast ions, and MHD modes, is further outlined in Sec. V A.

Next, we compare pulses #94701 and #95683 with a similar ICRF power ($P_{\text{ICRF}} \approx 6$ MW), but very different NBI power ($P_{\text{NBI}} = 8.1$ MW vs 18.4 MW). As seen in Figs. 7(a) and 7(c), the achieved neutron yield, $T_e(0)$ and the plasma stored energy are very similar, although there is a rather significant difference in the total auxiliary heating power (~ 14 MW vs ~ 24 MW). These results underline the decisive role of ICRF to accelerate ions to high energies and the associated fast-ion effects on the plasma, including neutron generation.

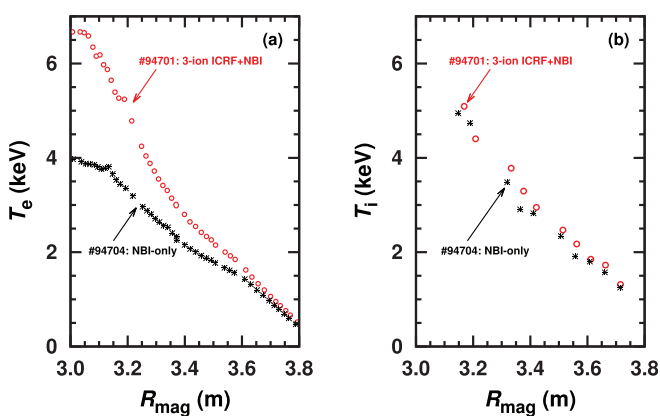


FIG. 9. Comparison of T_e (a) and T_i (b) profiles in JET pulses #94701 and #94704 at the same operational conditions and total auxiliary heating power, $P_{\text{aux}} \approx 14$ MW. Reprinted with stylistic modifications with permission from Kazakov *et al.*, Nucl. Fusion **60**, 112013 (2020). Reproduced courtesy of IAEA. Copyright 2020 EURATOM.

B. Efficient generation of passing fast ions and fast-ion current drive

Reversed-shear Alfvén eigenmodes (RSAEs)⁴³ were regularly observed in this series of fast-ion experiments in D-³He plasmas (3.7 T/2.5 MA) with $n(^3\text{He})/n_e \approx 20\%$ –25% and D-NBI ions as resonant absorbers. RSAEs were particularly pronounced during the phases with long-period sawteeth, sufficiently long to track the temporal evolution of the frequency of these modes, starting from the geodesic acoustic mode frequency (somewhat below ~ 100 kHz) up to the TAE frequency (~ 200 kHz). Figure 10 illustrates the excitation of RSAEs with toroidal mode numbers $n = 3$, $n = 2$ and $n = 1$ in JET pulse #94701 during the sawtooth cycle $t = 9.42\text{--}11.17$ s. To corroborate this result, we also show the excitation of RSAEs in the other JET pulse #95667 (Fig. 11) with a constant NBI power $P_{\text{NBI}} \approx 5.4$ MW and two levels of ICRF. The sawtooth period extended from $\Delta t_{\text{saw}} \approx 0.6$ s ($t = 7.83\text{--}8.44$ s) at $P_{\text{ICRF}} \approx 4.1$ MW up to $\Delta t_{\text{saw}} \approx 3.5$ s ($t = 8.44\text{--}11.94$ s) at $P_{\text{ICRF}} \approx 5.8$ MW. The bottom panel clearly illustrates the presence of RSAEs in this pulse as well. In particular, a very strong RSAE mode with $n = 1$ is seen in the Mirnov coil spectrogram. An interesting observation in #95667 is that the neutron rate is continuously increasing while the RSAE modes are seen and starts to decrease after the disappearance of the RSAEs. The regular observation of RSAEs in these experiments indicates that a nonmonotonic q -profile was developed and sustained during the application of the three-ion D-(D_{NBI})-³He scenario. Note that no RSAEs were seen in the heating phases with NBI-only.

In this section, we show that energetic D ions accelerated with the three-ion ICRF scenario in JET experiments remain co-passing ions. This is because of the combination of the strong localization of RF power deposition in the plasma core, nonstandard fast-ion orbit topology in that region and the quasilinear evolution of the fast ions. We note that the strong localization of RF power deposition and strong $|E_+|$ in a small volume is a particular feature of three-ion ICRF scenarios, when they are tuned for maximizing fast-ion generation in the plasma center of large devices such as JET. This was already shown for the three-ion D-(D_{NBI})-H scenario in Fig. 10 of Ref. 20, comparing the reconstructed neutron emission with the computed spatial

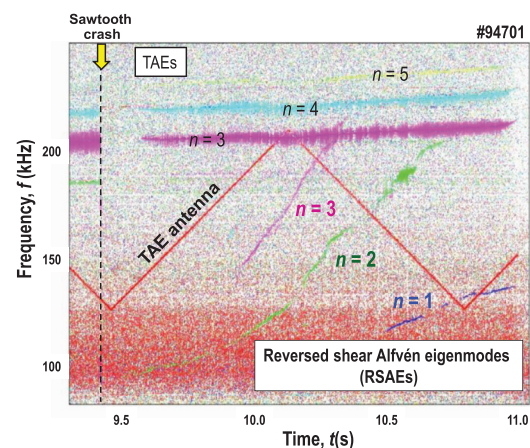


FIG. 10. Toroidicity-induced and reversed-shear Alfvén eigenmodes (TAEs and RSAEs) during the monster sawtooth phase in JET pulse #94701.

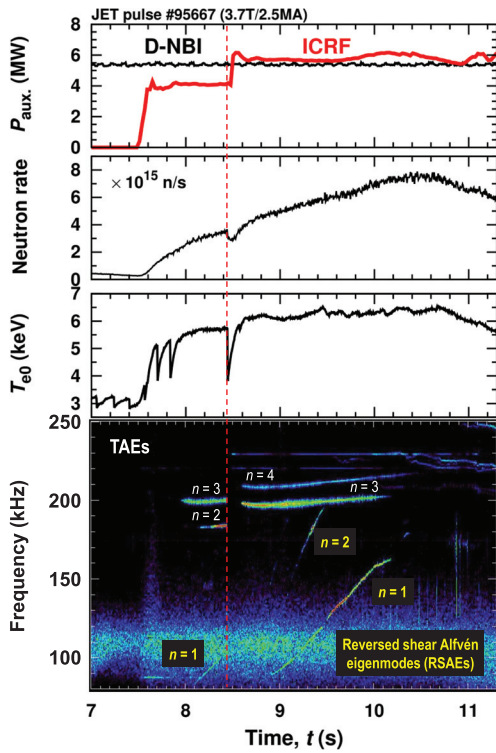
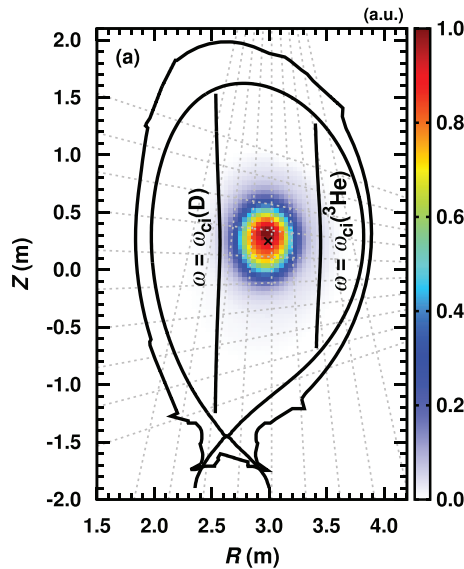


FIG. 11. Reversed shear Alfvén eigenmodes with $n=3$ (weak), $n=2$ and $n=1$ were observed in JET pulse #95667. The observation of RSAEs indicates that a nonmonotonic q -profile was developed and sustained when the three-ion D-(D_{NBI})-³He ICRF scenario was applied.



distribution of the RF electric field $|E_+|^2$ over the plasma cross section. This characteristic is further illustrated in Fig. 12(a) for the three-ion D-(D_{NBI})-³He scenario (JET pulse #94701), confirming the strong core localization of ICRF-accelerated fast D ions. The boundary separating trapped and passing ions is commonly given by the simplified expression $\lambda_* = \pm \sqrt{2r/(R_0 + r)}$,¹⁴ but this approximation is not valid here. In fact, as shown in Fig. 12(b), the trapped-passing boundary in the plasma region close to the magnetic axis has a very different structure (dashed lines) such that virtually all fast ions with $v_{||} > 0$ stay on co-passing orbits, even at high energies. This reasoning applies for both thermal and fast ions as resonant absorbers, accelerated by three-ion ICRF scenarios in JET.

To quantify this effect for three-ion ICRF scenarios with fast NBI ions as resonant absorbers we recall that according to the quasilinear theory,^{44–46} the cyclotron interaction of resonant ions with RF waves not only changes the energy of the particles, but also causes a change of their pitch and a displacement of their orbits. Because of the strong core localization of the fast-ion generation for centrally tuned three-ion ICRF scenarios, we ignore the orbit displacement effects and focus on analyzing how the pitch of the resonant ions changes as they are accelerated to MeV-range energies with ICRF. Following Refs. 45 and 46, we note that

$$\Delta\Lambda = (\Lambda_\infty - \Lambda)\Delta E/E, \quad (9)$$

where E is the kinetic energy, $\Lambda = \mu B_0/E$ is the normalized magnetic moment, $\Lambda = (1 - \lambda^2)B_0/B$, and $\Lambda_\infty = \omega_{ci}(0)/\omega$. With these approximations, one can easily derive from Eq. (9) that

$$\lambda(E) = \sqrt{\lambda_0^2 \frac{E_0}{E} + \lambda_\infty^2 \left(1 - \frac{E_0}{E}\right)}, \quad (10)$$

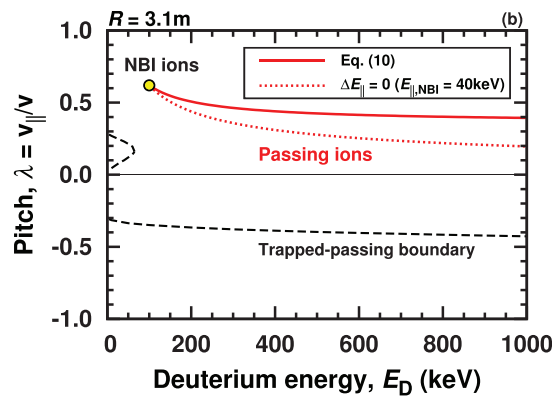


FIG. 12. (a) Strong core localization of neutron emission in JET pulse #94701. (b) The nonstandard trapped-passing boundary (dashed lines) in the plasma core facilitates the existence of passing fast ions with $v_{||} > 0$ in JET experiments. The solid line shows the estimated evolution of the pitch as a function of the fast-ion energy, Eq. (10). Resonant NBI ions with initial parameters $E_0 \approx 100$ keV and $\lambda_0 \approx 0.62$ remain on co-passing orbits during their RF-acceleration, as they stay spatially close to the magnetic axis.

with $\lambda_\infty^2 = 1 - \Lambda_\infty$; λ_0 and E_0 are the initial pitch and energy of resonant ions. Equation (10) provides an estimate for the change in the pitch of the resonant ions, as they absorb RF power and are accelerated to higher energies.

In these JET experiments in mixed H-D and D-³He plasmas using D-NBI ions as resonant absorbers,^{19,20,39} the IIF layer was on purpose located in the plasma core, in turn, implying that the cyclotron resonance for thermal D ions was positioned at the HFS off-axis (see Fig. 6), $\Lambda_\infty = \omega_{cD}(0)/\omega \approx 0.85\text{--}0.89$. Thus, according to Eq. (10), the asymptotic value of the pitch parameter of the ICRF-accelerated D ions reaches $\lambda_\infty \approx 0.34\text{--}0.38$. The evolution of the pitch-parameter of resonant ions as given by Eq. (10) is plotted with a red solid line in Fig. 12(b). The red dotted line shows the extreme (unphysical) case, where resonant NBI ions would only increase their perpendicular energy. Even then, the fast ions remain co-passing as a result of the unusual shape of the trapped-passing boundary in the plasma core.

This result is supported by TRANSP/TORIC simulations for the D-³He pulse #95679 in JET. Figure 13 shows the computed distribution function of the fast D ions in the core region of the plasma as a function of their pitch at $E_D = 100$ keV (blue dashed line, multiplied by a factor of 0.3) and at $E_D = 1.4$ MeV (red solid line with symbols). At the NBI injection energy, the population of fast D ions is peaked at $\lambda_0 \approx 0.62$. As follows from Fig. 13, at high energies $E_D = 1.4$ MeV most of the ICRF-accelerated D-NBI ions have a pitch in the range between 0.35 and 0.40. Thus, the analytical values predicted by Eq. (10) are in good agreement with TRANSP simulations. Furthermore, this important result is confirmed by gamma-ray measurements, as discussed in more detail in Ref. 39.

At first sight, it might look contradictory to generate significant RF-driven currents in three-ion ICRF + NBI experiments with a dipole ICRF antenna phasing, which has a symmetric k_{\parallel} -spectrum. Usually, asymmetric ICRF antenna spectra are used for localized fast-ion current drive, e.g., Ref. 47. However, the three-ion ICRF + NBI scenarios make use of the asymmetry in the v_{\parallel} -distribution of the

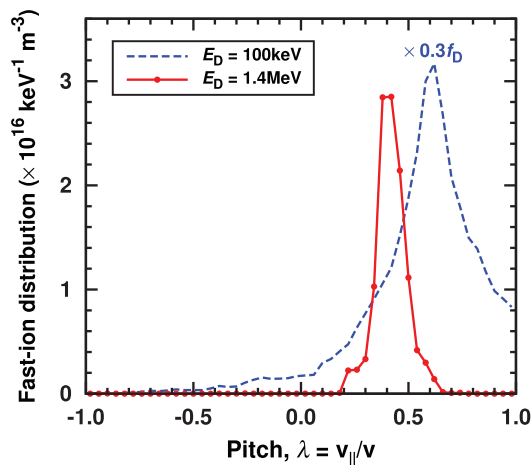


FIG. 13. Illustration of the computed distribution function of fast D ions in the core region of the plasma as a function of the pitch parameter for $E_D = 100$ keV (blue dashed line, multiplied by a factor of 0.3) and $E_D = 1.4$ MeV (red solid line with symbols). The computations were done by the TRANSP/TORIC code for the conditions of JET experiments in D-³He plasmas (pulse #95679).

resonant absorbers (D-NBI ions). Even when using dipole phasing, this results in preferential acceleration of fast ions in the co-current direction in JET. The systematic appearance of reversed shear AEs in these fast-ion experiments indicates that the q -profile in the core region is modified or even reversed. In addition to fast-ion current drive, other mechanisms associated with the application of the three-ion ICRF scenario could contribute here, as discussed in Sec. V B.

C. Toward ITER needs: Development of three-ion ICRF scenarios with off-axis heating on AUG and JET

Developing techniques to control edge localized modes (ELM) and reaching the ELMy H-mode are one of the main priorities for the nonactive ITER phase.⁴⁸ In hydrogen plasmas at half magnetic field (2.65 T/7.5 MA), reaching the ELMy H-mode may be challenging, partly due to the lack of an efficient ICRF absorption scenario in such plasmas.^{38,49,50} To bypass this limitation, ITER considers efficient ICRF scenarios at a toroidal field as close as possible to 2.65 T to reach the ELMy H-mode in hydrogen dominated plasmas. A possible solution is discussed in Ref. 51, where it was proposed to apply the three-ion ⁴He-(³He)-H scenario at the lowest available frequency of the ITER ICRF system, $f = 40$ MHz in H + 10%–15% ⁴He plasmas at $B_0 \approx 3.0\text{--}3.3$ T. Under these conditions, the cyclotron resonance of ³He ions is located at the HFS off-axis. It is important to demonstrate plasma heating with this off-axis scenario in present-day machines with a tungsten divertor such as AUG and JET. If successful, the proposed off-axis three-ion ICRF scenario would enable to provide an additional 20 MW for plasma heating. In turn, in combination with 33 MW of NBI and 20 MW heating with waves in the electron cyclotron range of frequencies (ECRF), this offers the potential to widen the H-mode operational space in predominantly hydrogen plasmas in ITER.

The first exploration of the three-ion ICRF scenario with HFS off-axis ³He heating was conducted in H-D plasmas, H/(H + D) ≈ 0.8 on AUG (2.5 T/0.8 MA; $f \approx 30$ MHz, dipole phasing). AUG has an all-tungsten (W) first wall and ICRF-specific W production has a strong influence on the application of high-power ICRF. The improved three-strap ICRF antennas are optimized to minimize W sputtering, in this way making ICRF compatible with a high-Z wall in AUG.^{52,53} Figure 14(a) shows an overview of the heating phase of the AUG pulse #35206, combining core ECRF (1.35 MW) and the three-ion ICRF scenario with off-axis heating. Adding ~ 1 MW of ICRF power resulted in a clear increase in the plasma stored energy and triggering the ELMy H-mode, seen in the signals for the divertor shunt currents and increase in the plasma density. Furthermore, the W concentration in the plasma, including the central region, stayed low $c_W < 2 \times 10^{-5}$ (measured by two diagnostics at the radial locations corresponding to $T_e \approx 1.5$ keV and $T_e \approx 3$ keV). As a next step, all three heating systems were combined on AUG, as foreseen for ITER, resulting again in good heating performance and low core W levels. For more details, see the description of AUG pulse #35207 in Ref. 54.

Very recently, a first attempt with the three-ion D-(³He)-H ICRF scenario with HFS off-axis ³He resonance was undertaken for plasma heating in H-D plasmas on JET-ILW. Figure 14(b) shows an overview of JET pulse #97084 (2.4 T/2 MA, $f = 32.2\text{--}33.0$ MHz), heated with $P_{\text{NBI}} = 8$ MW (deuterium) and complemented with $P_{\text{ICRF}} = 3$ MW starting from $t = 8.0$ s. A comparable increase in the plasma stored energy per MW of auxiliary heating power was observed for NBI and

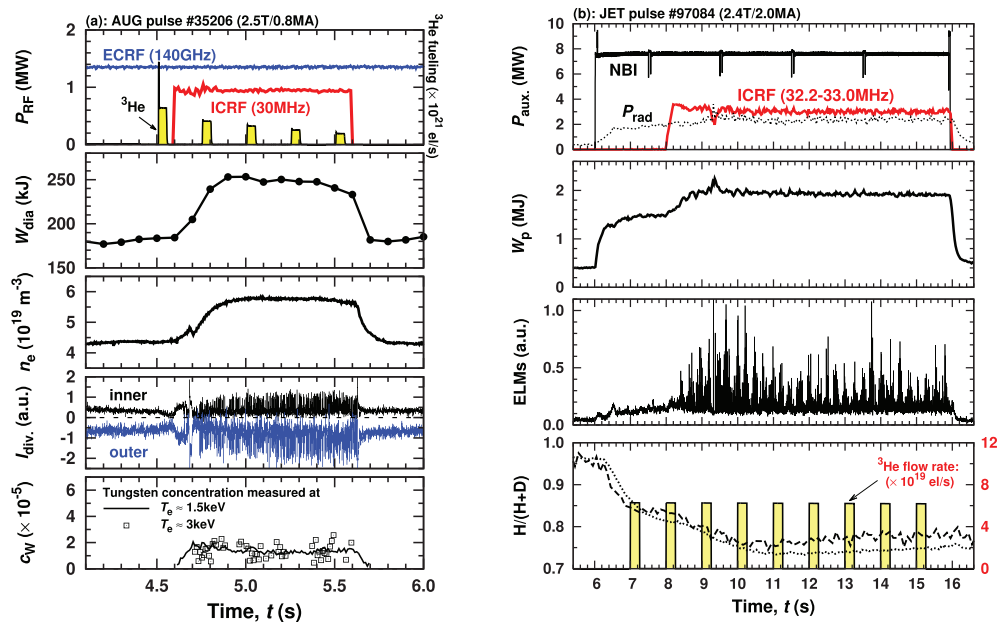


FIG. 14. Illustration of off-axis heating using the three-ion ICRF scenario with ^3He ions as resonant absorbers in mixed H–D plasmas on AUG (left: #35206, 2.5 T/0.8 MA, $f = 30$ MHz, dipole phasing) and JET-ILW (right: #97084, 2.4 T/2.0 MA, $f = 32.2$ – 33.0 MHz, dipole phasing), triggering L–H transitions and ELMy H-mode phases.

ICRF. In addition, the relative increase in the total radiated power before and after the application of ICRF, $\Delta P_{rad}/P_{ICRF}$ is less than 20% [see the evolution of the total radiated power, P_{rad} shown as a dotted line in the top panel of Fig. 14(b)]. For ITER it is important to demonstrate the three-ion ICRF scenario at the magnetic field as close as possible to 2.65 T. The conditions of JET pulse #97084 closely mimic the ITER heating scenario conditions at ~ 3.0 T. This first result is promising and more studies are foreseen in future experimental campaigns on JET.

In view of ITER needs, the next essential step was the demonstration of off-axis three-ion ICRF heating in nonactive H- ^4He plasmas. This was pioneered with success on AUG in the summer of 2019. The mix of heating systems on AUG (NBI, ECRF, and ICRF) uniquely mimics that of ITER. Figure 15 shows an overview of AUG pulse #36751 (2.5 T/0.8 MA, $n_{e0} \approx 4 \times 10^{19} \text{ m}^{-3}$) with a constant hydrogen NBI, $P_{H-NBI} = 0.8$ MW during the pulse. In the first phase of the pulse, the ECRF power was ramped up to 2.3 MW in order to trigger the L–H transition. In the second phase of the pulse with constant $P_{H-NBI} = 0.8$ MW and $P_{ECRF} = 0.8$ MW, ICRF power was added and ramped up to 1.6 MW, again leading to the L–H transition. This confirms that the mix of hydrogen NBI, ECRF, and ICRF using the three-ion scenario with off-axis deposition of RF power can also be applied to trigger ELMs in these ITER-relevant H- ^4He plasmas. Furthermore, L–H transitions and ELMy H-mode phases in H- ^4He plasmas were realized with ECRF + ICRF and ICRF-only on AUG. For this series of AUG experiments with off-axis three-ion ICRF heating, L–H transitions were generally reached at $P_{LH} \approx 2$ – 3 MW, which is similar to earlier observations with hydrogen NBI and ECRF heating in H- ^4He plasmas on AUG.⁵⁵ The fact that tungsten levels stayed low in these ICRF experiments on AUG is encouraging in view of possible application of this integrated heating scenario in ITER. Further studies of this

ITER-relevant heating scenario in H- ^4He and H–D plasmas are foreseen on AUG.

D. Optimization of fast-ion studies with three-ion ICRF scenarios on AUG

In AUG, the application of the three-ion ICRF scenario with on-axis ^3He resonance at extremely low concentrations, $n(^3\text{He})/n_e \approx 0.2\%$ did not show such clear signs of plasma heating as in JET. The reason for this difference is the reduced confinement of MeV-range ions in AUG, as compared to JET, because of the smaller machine size and smaller plasma currents. While JET is capable to confine most of the fast ^3He ions with energies of a few MeV, ^3He fast-ion energies in AUG should be limited to ~ 1 – 1.5 MeV to have sufficient time to transfer their energy to the background plasma during the slowing down. In order to reduce the energies of fast ^3He ions, and thus improve the confinement of the ICRF-heated ^3He ions on AUG, an obvious solution was to reduce the absorbed RF power per resonant ion.

Higher ^3He concentrations of $\sim 0.5\%$ – 1% were more optimal for on-axis heating of medium-size AUG plasmas. Figure 16(a) shows an overview of AUG pulse #34695 with the ^3He resonance on-axis (3.0 T/0.8 MA, $f = 30$ MHz, dipole phasing). This illustrates the increase in the plasma stored energy and plasma temperature after switching on the ICRF system at $t = 1.4$ s. The corresponding T_e and T_i profiles are shown in Fig. 16(b). Unfortunately, central electron temperature data are not available for AUG discharges at 2.8–3.0 T, making the analysis of the peakedness of the T_e profile rather difficult. The fact that energetic ^3He ions were sufficiently well confined in this pulse follows from the evolution of the plasma stored energy, increasing from 200 kJ in the NBI-only phase to ~ 300 – 310 kJ in the ICRF + NBI phase. Generation of energetic ^3He ions with on-axis ICRF resonance was

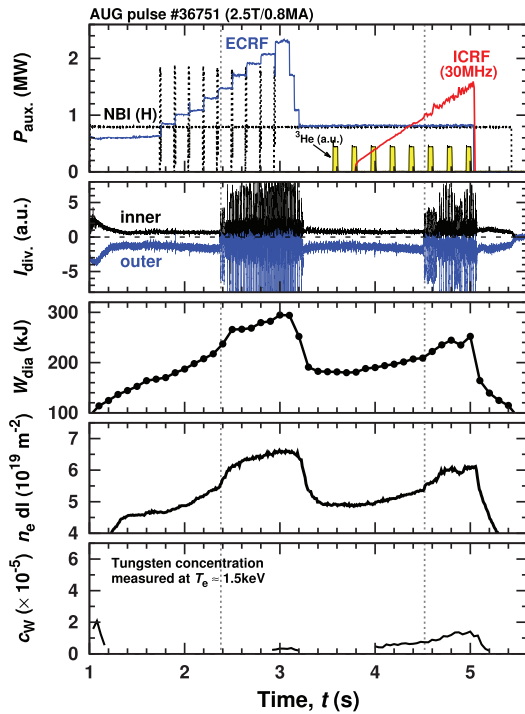


FIG. 15. AUG has prototyped the ITER-relevant heating scenario for nonactive H-⁴He plasmas with NBI, ECRF, and ICRF systems that has a potential to widen the H-mode operational space in ITER. This example illustrates how a ramp of ICRF power using the three-ion ⁴He-(³He)-H scenario with off-axis RF power deposition was applied to trigger ELMs in AUG pulse #36751 (2.5 T/0.8 MA). The vertical dotted lines correspond to the L–H transitions and the appearance of ELMs.

also observed in AUG plasmas, confirmed by the excitation of Alfvénic modes ($f_{AE} \approx 160\text{--}190\text{ kHz}$), the appearance of fishbones and by fast-ion loss detector (FILD) measurements, shown in Fig. 17(a). The backward-orbit tracing of escaping ions measured by FILD was undertaken for H, D and ³He ions, as shown in Figs. 17(b)–17(d), and infers that the measured escaping ions originate from the plasma core. The backward-traced orbits for energetic ³He ions are consistent with

the ³He ICRF resonance located in the plasma core. The fast-ion energies can be estimated using the following formula:

$$E_i(\text{MeV}) = \left(\frac{\rho_L(\text{cm})B_{\text{FILD}}(\text{T})}{14.45} \right)^2 \frac{Z_i^2}{A_i}, \quad (11)$$

where ρ_L is the Larmor radius of escaping ions measured by FILD and B_{FILD} is the magnetic field strength at the position of the detector. Using Eq. (11) with $B_{\text{FILD}} \approx 2.3\text{ T}$ for #34695, one finds that the measured fast ions with $\rho_L = 7\text{ cm}$ correspond to ³He ions with energies of $\sim 1.7\text{ MeV}$.

Alternatively, one can also reduce the energies of the generated fast ³He ions by shifting the resonance location off-axis. In this way, the same amount of RF power is deposited in a larger volume, thus, reducing RF power per resonant ion. This was applied successfully in AUG pulse #34704 ($n(^3\text{He})/n_e \approx 0.5\% \text{--} 1\%$) by reducing the toroidal magnetic field to 2.8 T and shifting the ³He cyclotron resonance to $\rho_{\text{pol}} \approx 0.3$ at the HFS. As shown in Fig. 18, ICRF power was increased in three steps: 0.9 MW, 1.9 MW, and 2.5 MW. Consequently, the plasma stored energy increased from $\sim 300\text{ kJ}$ during the NBI-only phase with $P_{\text{NBI}} = 8\text{ MW}$ to $\sim 400\text{ kJ}$ during the ICRF + NBI phase. The TORIC-SSFPQL modeling⁵⁶ of this pulse showed that the perpendicular temperature of RF-heated ³He ions reached $\sim 500\text{ keV}$ in the phase with $P_{\text{ICRF}} = 2.5\text{ MW}$, see Refs. 57 and 58. A gradual increase in T_e measured at $\rho_{\text{pol}} \approx 0.2$ seen in Fig. 18 is consistent with the fact that energetic ³He ions transfer most of their energy during their slowing-down to the electrons. CXRS measurements confirmed the presence of confined energetic ³He ions in the plasma.^{57,58} The magnitude of the predicted charge exchange spectral radiance, obtained via forward-modeling of the spectrum utilizing TORIC-SSFPQL distribution functions, and the expected energies of the ions agree well with the measurement, confirming that the spectral feature is due to ICRF-accelerated ³He ions, as reported in Ref. 58.

These examples illustrate that three-ion ICRF scenarios at very low concentrations of resonant absorbers can be effectively used to probe the limits of fast-ion confinement in fusion devices. Indeed, our experience with the development of on-axis heating of AUG plasmas with this scenario highlights that it can easily generate fast ions that are too energetic to be confined in this tokamak. Therefore, pushing for the maximum efficiency of fast-ion acceleration [e.g., on-axis ICRF resonance and very low $n(^3\text{He})/n_e$] in smaller-size machines does not necessarily maximize the number of confined fast ions in the plasma and,

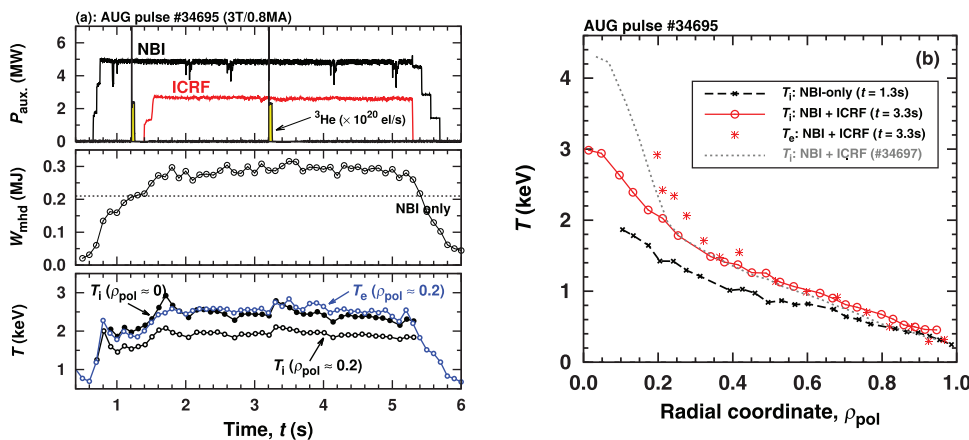


FIG. 16. (a) Overview of AUG pulse #34695 with on-axis ³He resonance (3.0 T/0.8 MA, $f = 30\text{ MHz}$, dipole phasing). (b) T_e and T_i profiles in #34695.

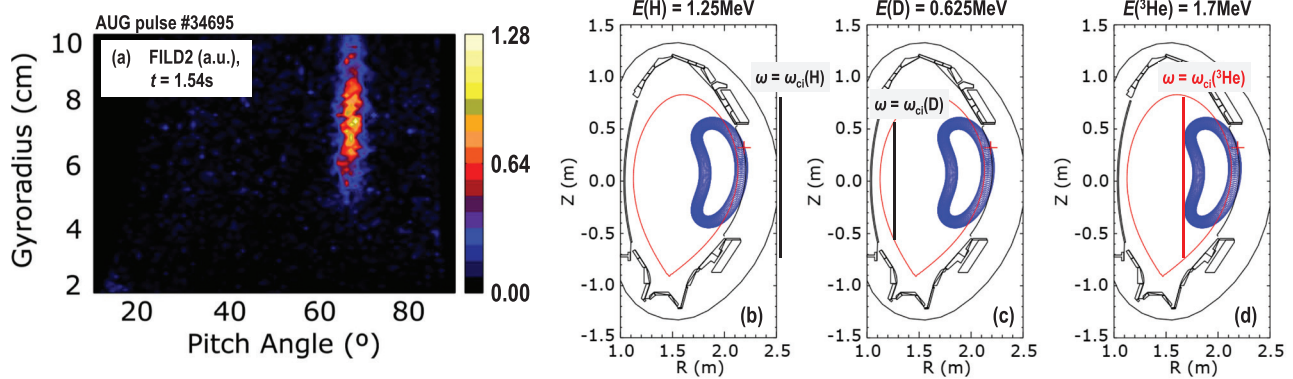


FIG. 17. (a) FILD analysis for AUG pulse #34695 with on-axis ^3He resonance. (b)–(d) Backward-orbit tracing of escaping ions, assuming H, D, and ^3He ions entering the FILD detector. Reprinted with permission from Meyer *et al.*, Nucl. Fusion **59**, 112014 (2019). Reproduced courtesy of IAEA. Copyright 2019 EURATOM.

in fact, can lead to disappointing results. In such a case, a careful optimization of the scenario parameters (e.g., plasma composition, resonance location, antenna phasing, etc.) is needed to maximize the content of confined fast ions.

IV. A COMMON FRAMEWORK TO EXPLAIN EARLIER EXPERIMENTAL RESULTS WITH ICRF HEATING IN MIXED PLASMAS

A. Unexpected RF power absorption by impurities in D-T experiments in TFTR and JET

In TFTR, the success of mode conversion experiments for localized electron heating and current drive in D- ^3He plasmas motivated the team to apply this ICRF scenario also in D-T plasmas.

However, in the experiments only $\sim 20\%$ of the incoming RF power heated the electrons, in contrast to what was expected, see Fig. 19 (reprinted from Ref. 21). The low efficiency of mode conversion electron heating was attributed to the presence of a small amount of ^7Li ions, $n(^7\text{Li})/n_e \approx 0.5\%$, absorbing most of the launched RF power. The ^7Li ions originated from the use of natural lithium pellets (note that ^7Li constitutes 92.5% of naturally occurring lithium) to condition the TFTR wall in those D-T experiments. Supported also by numerical modeling, it was soon realized that $\sim 80\%$ of RF power was absorbed by ^7Li ions, despite their low concentrations. In fact, the three-ion T-(^7Li)-D ICRF scenario was effectively at work and ^7Li ions absorbed RF power near one of the IHH layers located close to the cyclotron resonance of ^7Li .

In their paper,²¹ the authors discussed all essential elements, in particular, the enhanced left-hand RF polarization at the IHH layer, and explained the mechanism behind the observed strong impurity absorption. However, as the ICRF resonance of the ^7Li ions was located LFS off-axis for the chosen conditions, the absorption was considered a parasitic effect, preventing the RF power to reach the

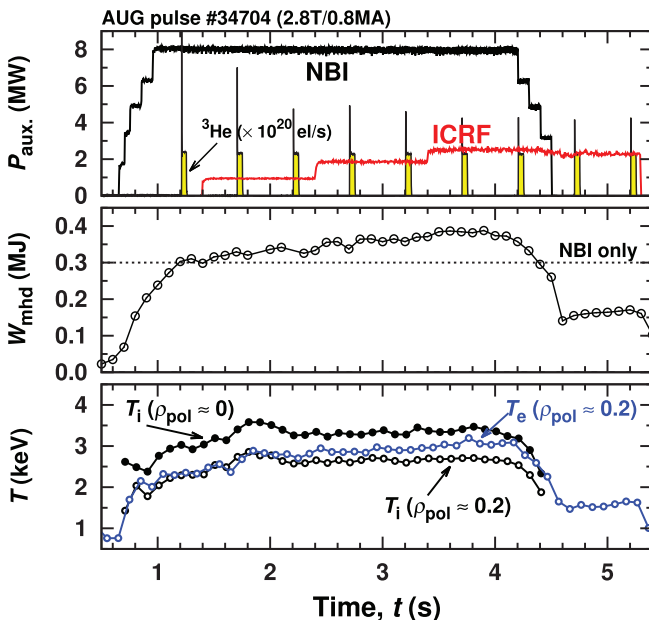


FIG. 18. Overview of AUG pulse #34704 (2.8 T/0.8 MA, $f = 30$ MHz, dipole phasing) with HFS off-axis ^3He resonance at $\rho_{\text{pol}} \approx 0.3$.

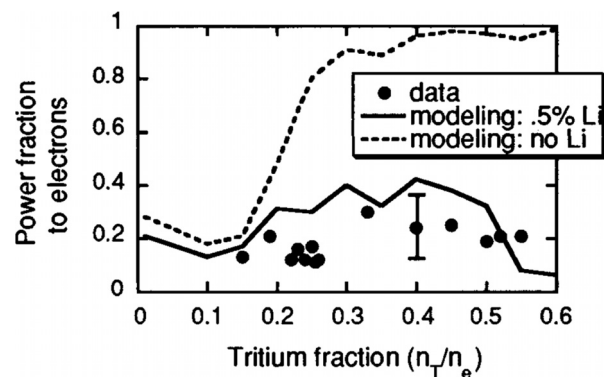


FIG. 19. TFTR mode conversion experiments in D-T plasmas: expectation vs reality. While the experimental conditions were set for core electron heating via mode conversion, experimental results surprisingly showed that most of the RF power was absorbed off-axis before reaching the plasma core. Reproduced with permission from Wilson *et al.*, Phys. Plasmas **5**, 1721 (1998). Copyright 1998 AIP Publishing.

plasma core. To eliminate this unwanted ${}^7\text{Li}$ absorption, isotopically ${}^6\text{Li}$ -enriched pellets were used in the next series of D–T experiments and electron mode conversion heating was recovered. As ${}^6\text{Li}$ ions have the same $Z/A = 1/2$ ratio as D ions, they cannot act as a third resonant absorber in D–T plasmas.

Tungsten and beryllium have been chosen as the plasma-facing components for JET-ILW and ITER, resulting in a non-negligible amount of ${}^9\text{Be}$ impurities in the plasma. In JET-ILW, typical concentrations of ${}^9\text{Be}$ are usually about $\sim 0.5\%$ – 1% . In their publication,²¹ the TFTR team also correctly highlighted that strong ICRF damping on ${}^9\text{Be}$ impurities will arise in ITER D–T plasmas, and that this would lead to effects similar to their observations with ${}^7\text{Li}$. However, our developments show that the unwanted “parasitic” absorption by ${}^7\text{Li}$ and ${}^9\text{Be}$ ions could be easily converted into an efficient scenario for bulk ion heating in JET-ILW and ITER D–T plasmas.^{26,59,60}

Another important outcome of the analysis by the TFTR team was the conclusion that mode conversion heating in D–T plasmas in the frequency range $\omega_{cT} < \omega < \omega_{cD}$ is not consistent with ${}^9\text{Be}$ plasma-facing components, unless the level of ${}^9\text{Be}$ can be kept very low.²¹ Indeed, as follows from detailed numerical analysis for ITER in Ref. 59, already at ${}^9\text{Be}$ concentrations as low as $\sim 0.1\%$ – 0.2% most of RF power will be absorbed by these intrinsic impurities via the three-ion T-(${}^9\text{Be}$)-D scenario, thereby preventing mode conversion heating in D–T = 50%–50% plasmas and thus also the use of mode converted ion Bernstein waves (IBW) for other applications.

There was a similar puzzling observation in D–T ICRF experiments in JET with the carbon wall, when the deuterium concentration was varied between 9% and 22%.⁶¹ It was reported that while the largest fusion yield was reached at 9% of D, strong bulk ion heating occurred at 18% of D, with a $\sim 60\%$ contribution from the thermal fusion reactions to the total neutron yield. Strong ICRF damping on $\sim 1.5\%$ ${}^9\text{Be}$ impurities in D–T plasmas, amplified by the large E_+ at the IIH layer, was put forward as one of the possibilities to explain the observations. The conclusion was that under those experimental conditions, ${}^9\text{Be}$ impurities can absorb up to 40% of the incoming RF power. In fact, all the essential elements for the three-ion ICRF scenario in D–T plasmas with ${}^9\text{Be}$ as resonant absorbers were described in Ref. 61. We note that in D–T = 50%–50% plasmas ICRF power absorption by ${}^9\text{Be}$ impurities is even more effective.

B. Efficient acceleration of D-NBI ions in D- ${}^3\text{He}$ mode conversion experiments in JET-C and TFTR

A competing damping mechanism was observed in D- ${}^3\text{He}$ ICRF mode conversion experiments with $n({}^3\text{He})/n_e \approx 25\%$ – 35% on JET with the carbon wall (JET-C), in the presence of fast D-NBI ions ($E_{\text{NBI}} \approx 135$ keV). At such large ${}^3\text{He}$ concentrations (above the optimal one for mode conversion), energetic D ions were observed, evidenced by the strong increase in the neutron yield, the intensity of the gamma-rays and long neutron decay times after the D-NBI blip: see Sec. 2.2 in Ref. 12 for a detailed discussion. This effect was also later observed in JET-C ICRF experiments in D- ${}^3\text{He}$ plasmas with $n({}^3\text{He})/n_e \approx 20\%$, as reported in Ref. 28.

It is well known that mode converted IBWs are characterized by much larger perpendicular wavenumbers than fast waves. As a result, interaction between ions and IBWs cannot lead to the generation of populations of MeV-range ions. Thus, the clear experimental

observation of fast D ions with energies significantly above the NBI injection energy is proof of an efficient transfer of RF power from the launched fast waves rather than from mode converted IBWs. Fulfilling the resonance condition, Eq. (1) for fast D-NBI ions at the IIH layer was realized by the authors of Ref. 12 as the mechanism responsible for the observed efficient generation of high-energy D ions. In one of the comparison shots, the ${}^3\text{He}$ puff was replaced by a similar ${}^4\text{He}$ puff, resulting in a strong reduction of the ${}^3\text{He}$ concentration and an associated shift of the IIH layer. Thus, the fast D-NBI ions were no longer resonating at the IIH layer, leading to the disappearance of highly energetic D ions in the plasma.

Note that similar observations were also made in ICRF experiments in D- ${}^3\text{He}$ plasmas on TFTR⁶² in the presence of D-NBI heating. At large $n({}^3\text{He})/n_e \approx 20\%$ strongly enhanced fast-ion losses were observed, considered to be either D–D fusion-born tritons or ICRF-accelerated D-NBI ions. The results of our recent JET-ILW experiments in D- ${}^3\text{He}$ plasmas proved that D-NBI ions can be effectively accelerated to high energies by the launched fast waves in the vicinity of the IIH layer. As follows from ICRF modeling, at these conditions only a few % of the incoming RF power reaches the point where fast waves undergo mode conversion to IBWs.

In fact, recent fast-ion studies in JET-ILW D- ${}^3\text{He}$ plasmas with $n({}^3\text{He})/n_e \approx 20\%$ – 25% using the three-ion D-(D_{NBI})- ${}^3\text{He}$ scenario, as described in Secs. III A and III B, is a natural follow-up of those earlier experiments in JET-C and TFTR. The enhanced set of fast-ion diagnostics now available at JET, combined with the progress with the development of heating and transport modeling codes, allows a much more detailed understanding of the complex physical processes, taking place in these mixed D- ${}^3\text{He}$ plasmas.

C. The importance of residual D ions and intrinsic carbon impurities for ${}^3\text{He}$ ICRF experiments in H plasmas on AUG and JET with a carbon wall

A series of ${}^3\text{He}$ minority and mode conversion experiments in H majority plasmas were undertaken on the AUG and JET tokamaks, both with a carbon wall at the time of the experiments.^{15,63–65} Both studies highlighted that for the correct interpretation of the experimental results, including the presence of additional ion species with $(Z/A) = 1/2$ is essential. All ions with $(Z/A) = 1/2$ contribute to an equivalent total concentration of D ions

$$X[\text{D}]_{\text{equiv.}} = X[\text{D}] + 2X[{}^4\text{He}^{2+}] + 6X[{}^{12}\text{C}^{6+}] + \sum_{\text{imp}} Z_{\text{imp}} X_{\text{imp}}, \quad (12)$$

where the contributions from D, ${}^4\text{He}^{2+}$, and ${}^{12}\text{C}^{6+}$ ions are explicitly taken into account, and the last term includes the sum over all other ion species in the plasma with $Z/A = 1/2$. In ICRF experiments on AUG with the carbon wall,⁶³ the concentration of residual D ions was $\sim 15\%$. Similar equivalent concentrations of D ions ($X[\text{D}]_{\text{equiv.}} \approx 14\%$ – 20%) were reached in ICRF experiments in JET-C plasmas¹⁵ that contained $\sim 2\%$ – 3% of intrinsic carbon impurities and $\sim 2\%$ of residual deuterium. Thus, from the ICRF point-of-view, those plasmas were equivalent to an H–D mix with $n(\text{D})/n_e \approx 15\%$ – 20% and correspondingly $n(\text{H})/n_e \approx 80\%$ – 85% .

In fact, the isotopic H–D ratio in recent three-ion ICRF experiments on Alcator C-Mod, JET and AUG with resonant ${}^3\text{He}$ ions

closely mimicked the conditions achieved in earlier ^3He ICRF experiments in hydrogen plasmas on AUG and JET-C. The authors of Refs. 15 and 63–65 clearly realized and highlighted the importance of residual D ions and carbon impurities, and their impact on the details of RF wave propagation and power absorption under those experimental conditions. New developments highlight the potential to exploit the presence of intrinsic and extrinsic impurities in the plasma, as an active element to control ICRF power deposition and fast-ion generation.

V. PROMISING APPLICATIONS FOR FUSION RESEARCH

As follows from the discussions in Secs. II–IV, for almost any mixed plasma, including D–T, one can find a corresponding three-ion ICRF scenario for a specific task. This section describes practical applications of these novel ICRF scenarios beyond plasma heating and fast-ion generation, which have a promising potential for fusion research, but are still largely under development.

A. A tool for the fast-ion driven MHD modes and turbulence studies

Dominant core electron heating from fusion-born alphas will be the main source of plasma heating in future D–T experiments. Recent theoretical studies highlight that alpha particles can significantly stabilize ITG turbulence and reduce heat transport in ITER.⁶⁶ Thus, developing heating scenarios in present-day tokamaks that closely mimic the conditions of fast-ion electron heating representative for ITER plasmas is very important to obtain a deeper understanding of the expected impact of the fusion-born alphas in D–T plasmas and validate existing state-of-the-art microturbulence codes with the data obtained.

Furthermore, fusion-born alpha particles in D–T plasmas in ITER are expected to destabilize Alfvén eigenmodes, possibly leading to detrimental effects on plasma confinement.⁶⁷ In view of ITER, several fast-ion scenarios have been developed on different machines in recent years to excite AE modes and study the mechanisms for their control.⁶⁸ As discussed in Sec. III A, a large variety of Alfvénic modes such as TAEs, RSAEs, and EAEs are regularly observed in JET experiments with three-ion ICRF scenarios optimized for core heating and fast-ion generation, see Fig. 8.

Surprisingly, in most cases, the observed complex AE activity was not detrimental for plasma confinement in three-ion ICRF studies on JET. Recent gyrokinetic analysis of these experiments in D– ^3He plasmas and its comparison with the NBI-only pulse #94704 highlights that efficient ion heating can be reached in the presence of MeV-range fast ions and fully destabilized TAEs seen experimentally through a complex multi-scale mechanism that generates intense zonal flows.⁴¹ This mechanism is promising to reach high T_i in future fusion plasmas with strong electron heating by the alpha particles. Note that the suppression of the electrostatic turbulence with moderately energetic fast ions (~ 100 keV) in the presence of marginally stable TAEs, appearing in the gyrokinetic GENE simulations, was discussed in Ref. 69.

B. A tool to modify the q -profile in the plasma core

Reversed-shear Alfvén eigenmodes were regularly observed in JET experiments with the three-ion ICRF scenario in D– ^3He plasmas,

as discussed in Sec. III B (see also Figs. 10 and 11). This indicates that the application of this fast-ion scenario with associated phenomena led to a modification of the q -profile. Several mechanisms could contribute. First, three-ion ICRF scenarios on JET generate a population of co-passing fast D ions and fast-ion current drive, but not necessarily peaked exactly on-axis. This could be caused by, e.g., the Shafranov shift of the magnetic axis and variations of the plasma composition, defining the exact location of the IIIH layer. Second, the significantly higher T_{e0} reached during the phases with ICRF increases the number of fast ions in the slowing-down population as $n_{\text{fast}} \propto T_e^{3/2}$ [e.g., in pulse #94701 T_{e0} doubled from ~ 3.5 keV during NBI-only to ~ 7.0 keV during the combined ICRF + NBI phase, see Fig. 7(a)]. Furthermore, the strongly peaked pressure profile also leads to an increased bootstrap current contribution. All these simultaneously appearing effects are a direct consequence of the application of the three-ion ICRF scenario. The detailed understanding of the interplay between various mechanisms, leading to systematic observations of RSAEs, is a subject of ongoing active research. In this context, it is important to mention that RSAEs were also observed in three-ion ICRF experiments on JET in H–D (and very recently in H– ^4He) plasmas with thermal ^3He ions as resonant absorbers, when using co-current drive ICRF antenna phasing. These experimental results illustrate that three-ion ICRF scenarios have the potential to become a control tool to modify the q -profile in the central region of the plasma.

C. Bulk ion heating in D–T plasmas

Second harmonic heating of tritium ions is considered as the main ICRF scenario for D–T plasmas in ITER, facilitated by the injection of a few percent of ^3He ions to maximize bulk ion heating and to increase T_i during the ramp-up phase of the pulse. Because ^3He is a scarce gas, using the three-ion T–(^9Be)–D scenario with a small amount of intrinsic ^9Be impurities ($\sim 1\%$) as resonant absorbers was proposed for RF heating in D–T = 50%–50% plasmas.⁵⁹ In fact, ^9Be impurities are the dominant channel of RF power absorption for a fairly broad D:T range, as shown by numerical simulations in Ref. 59. As follows from basic Coulomb collision theory, ^9Be impurities have a substantially larger critical energy than ^3He ions, viz., $E_{\text{crit}}(^9\text{Be}) \approx 74 T_e$ vs $E_{\text{crit}}(^3\text{He}) \approx 25 T_e$, and thus transfer an even larger fraction of absorbed RF power to bulk D and T ions, as illustrated in Table I of Ref. 59. This ICRF heating scenario is compatible with additional seeding of Ar and ^{22}Ne impurities (candidate ions for impurity seeding in ITER and future reactors⁷⁰) having a very similar charge-to-mass ratio as ^9Be .

We note the potential of intrinsic impurities with $1/3 < (Z/A) < 1/2$, such as ^7Li and ^9Be , to absorb RF power efficiently in D–T plasmas was already experimentally observed at TFTR and JET,^{21,61} as discussed in Sec. IV A. Essentially, new insights suggest that instead of considering this effect as a parasitic impurity absorption, it can be used to the benefit of future studies in D–T plasmas in JET-ILW and ITER.^{26,59}

D. Revisiting the parasitic absorption by alphas in D–T plasmas

ICRF heating of JET-ILW and ITER D–T plasmas with intrinsic ^9Be plasma impurities in the frequency range $\omega \approx \omega_{\text{cD}}$ and below is generally quite efficient as different resonant ion populations can

absorb RF power at different radial locations. These include thermal D and T ions, ${}^9\text{Be}$ and other impurities with $1/3 < (Z/A) < 1/2$, injected fast D-NBI or T-NBI ions and fusion-born alpha particles. The exact split of the absorbed RF power between these components depends on the details of the selected operational settings, including the D:T ratio, ICRF and NBI parameters, plasma density and temperature, concentration of impurities, the amount of fusion-born alphas, etc.

For example, at $n(\text{D})/n_e \approx 10\%$, RF power is efficiently absorbed by thermal D and fast D-NBI ions in the vicinity of the D cyclotron resonance, $\omega \approx \omega_{\text{CD}}$ and at the LFS of it. In the absence of D-NBI, the high efficiency of the D minority heating scenario was demonstrated in past ICRF experiments in D-T plasmas on JET.⁶¹ In combination with high power D-NBI, this ICRF scenario has been proposed to reach high fusion power in future D-T experiments in JET-ILW.^{60,71}

At higher concentrations of D ions $n(\text{D})/n_e \approx 20\%–30\%$, RF power absorption at $\omega \approx \omega_{\text{CD}}$ becomes less efficient. A large amount of the RF power, launched from the LFS, can pass through the region $\omega \approx \omega_{\text{CD}}$ and reach the IHH layers in D-T plasmas, thus allowing to make use of the three-ion scenarios. Due to the unavoidable presence of ${}^9\text{Be}$ impurities in JET-ILW and ITER plasmas, one of the IHH layers is located in close proximity to the cyclotron resonance of ${}^9\text{Be}$, facilitating RF power absorption by these impurities. Furthermore, simultaneously fast D-NBI ions and alpha particles can absorb RF power in the vicinity of this IHH layer ($k_{\parallel}v_{\parallel} < 0$), thereby exploiting the advantages offered by the three-ion ICRF scenarios. To control the exact split of the RF power between the various resonant absorbers, different antenna phasings with different dominant values of k_{\parallel} can be applied.

Absorption of ICRF power by fusion-born alpha particles in D-T plasmas is usually considered as a parasitic effect to be avoided.^{72,73} The higher the plasma temperatures, the more fusion-born alpha particles are present in the plasma, leading to increased amount of RF power absorbed by these alphas and consequently reduced ICRF power absorption by ${}^9\text{Be}$ and other heavy impurities. As discussed in Secs. III B and V B, generating passing fast ions in the central regions of the plasma can be used as a tool to modify the q -profile. As the alpha distribution in D-T plasmas in ITER is to a large extent isotropic in v_{\parallel} ,⁶⁷ an asymmetric k_{\parallel} antenna spectrum is required to generate a net noninductive current by the fusion-born alpha particles. Choosing an ICRF antenna phasing to launch RF waves predominantly in the co- or counter-current direction might potentially be used as an additional actuator allowing to reverse the direction of the alpha-driven current. Thus, using parasitic absorption of ICRF power by alphas in the vicinity of the IHH layers in D-T plasmas might offer the potential to contribute to the control of the shape of the q -profile in the central region of the plasma. As, in turn, the q -profile is known to impact the global plasma confinement, this opens an additional promising application for ICRF as a control system in high-temperature D-T plasmas.

E. Complementary scenarios to demonstrate alpha particle effects in future D-T experiments on JET

One of the main objectives of the forthcoming D-T campaign on JET (DTE2) is to demonstrate and study the effects associated with the presence of fusion-born alpha particles.^{74,75} To achieve this task, JET is developing a dedicated scenario to excite alpha-driven AEs in the afterglow phase of high-performance D-T plasmas with internal transport barriers, heated with NBI-only.⁷⁶

The success with the development of three-ion ICRF scenarios in H-D and D- ${}^3\text{He}$ plasmas on JET opens new promising routes for demonstrating alpha effects in JET-ILW. In particular, we note the ongoing effort for designing a dedicated scenario to demonstrate alpha particle heating in DTE2, in which fusion-born alphas provide the main source of electron heating in the plasma core and where the post-sawtooth reheat rate, $dT_e(0)/dt$ is used as a figure-of-merit to characterize electron heating power densities in the plasma core.⁷⁷ In this context, applying three-ion ICRF scenarios with heavier impurities as resonant absorbers (${}^9\text{Be}$, possibly in combination with Argon or ${}^{22}\text{Ne}$) is promising as they collisionally transfer most of the absorbed RF power to bulk ions and thus minimize core electron heating from ICRF. Equally important, these heavy resonant ions stay at sub-Alfvénic velocities and thus are less likely to trigger AEs even at MeV-energies.

In addition, three-ion ICRF scenarios with fast T-NBI or D-NBI ions as resonant absorbers are also promising for their use in DTE2. As we demonstrated the possibility to control the fast-ion distribution with the ratio $P_{\text{ICRF}}/P_{\text{NBI}}$ and the choice of NBI injectors, this technique offers JET the possibility to accelerate NBI ions with ICRF to energies, for which the D-T reactivity is maximized, as proposed in Ref. 19. In this way, this technique can be used to optimize the alpha production and beam-target neutron rate in D-T plasmas at moderate input heating power. Similar to the D- ${}^3\text{He}$ experiments discussed in Sec. III A, rather high alpha generation rates can thus be obtained for a moderate total auxiliary heating power. In combination with the off-axis location of the IHH layer and beam heating, the energies of ICRF-accelerated fast ions can be controlled to be below or comparable to the critical energy. Thus, this scenario can facilitate the design of dedicated experiments to demonstrate alpha physics effects in JET-ILW.

F. Extending H-mode access in hydrogen majority plasmas in ITER

Access to ELMy H-mode plasmas and developing ELM control techniques are one of the main priorities for ITER studies with nonactive plasmas.⁴⁸ Partly due to the lack of an efficient ICRF absorption scenario in hydrogen plasmas at half magnetic field (2.65 T/7.5 MA), this may be challenging for such plasmas. For H-mode access, the difference in the total auxiliary heating power available, 53 MW (NBI + ECRF) vs 73 MW (NBI + ECRF + ICRF), could well be essential. Thus, an alternative heating scenario with all three heating systems of ITER was proposed in Ref. 51. This relies on using the mix H + 10%–15% of ${}^4\text{He}$ ions (shown to reduce the L-H power threshold in NBI-only heated plasmas in JET-ILW⁷⁸) and increasing the nominal magnetic field to 3.0–3.3 T. In these plasmas, the three-ion ${}^4\text{He}$ -(${}^3\text{He}$)-H ICRF scenario with an off-axis ${}^3\text{He}$ resonance [$n({}^3\text{He})/n_e < 1\%$] is capable to provide an additional 20 MW of heating power to the plasma. Thus, this heating scenario has the potential to extend the H-mode operational space in predominantly hydrogen plasmas in the PFPO-2 phase of ITER.^{38,51}

As discussed in Sec. III C, in view of ITER needs, promising results have been recently obtained on AUG and JET. Particularly relevant are the pioneering results with the off-axis three-ion ${}^4\text{He}$ -(${}^3\text{He}$)-H ICRF scenario in H- ${}^4\text{He}$ plasmas on AUG, in which all three heating systems were used. The simultaneous realization of plasma heating with ICRF, ICRF-triggered L-H transitions, and low levels of impurities is encouraging. Further studies of this ITER-

relevant three-ion ICRF heating scenario in nonactive H-⁴He plasmas and further optimizations are foreseen in future campaigns on AUG and JET.

G. Using impurities as an active tool to control RF polarization and ICRF absorption

The role of low-*Z* impurities in multi-ion species plasmas can go beyond being an absorber of RF power, as for ⁹Be and ⁷Li ions in D-T plasmas. Low-*Z* impurities can also provide a significant contribution to the RF polarization, as, e.g., for the carbon impurities during ³He ICRF experiments in hydrogen plasmas in JET with the carbon wall,^{15,64,65} discussed in Sec. IV C. Yet nothing prevents extending this idea and using a combination of intrinsic and extrinsic impurities as an active tool to control polarization and deposition of RF waves.

Because of the unavoidable presence of ⁹Be impurities in ITER and JET-ILW plasmas, neither pure (⁴He)-H, nor (D)-H minority scenarios can be realized in these machines. Because $(Z/A)_{9\text{Be}} < (Z/A)_{4\text{He}} < (Z/A)_{\text{H}}$, ⁹Be impurities are not resonant absorbers in these plasmas, but are a crucial component that defines the polarization of RF waves and, thus, impacts RF heating of resonant ⁴He ions.^{17,79} This is illustrated in Fig. 20, where the fraction of RF power absorbed by resonant ⁴He ions is plotted as a function of both $n(^9\text{Be})/n_e$ and $n(^4\text{He})/n_e$, computed by the full-wave TORIC code.³⁵ It is very clear that power absorption by ⁴He can vary from 0% to 100%, depending on the plasma composition. For example, if $n(^9\text{Be})/n_e > 3\%$, then ICRF heating of ⁴He ions becomes a very poor heating scenario with unwanted strong fast wave reflections. Figure 20 shows that efficient ICRF absorption by ⁴He ions at very low concentrations ($\sim 0.2\%$) is maximized at $n(^9\text{Be})/n_e \approx 1.5\% - 2.5\%$, in line with the theoretical formulas for the three-ion ⁹Be-(⁴He)-H scenario [Eq. (5)]. These conditions are

beneficial if one aims to generate MeV-range ⁴He ions in hydrogen majority plasmas, e.g., to validate fast-ion diagnostics.

As controlling the concentration of ⁹Be intrinsic impurities ($Z/A = 4/9$) in the plasma is not straightforward, using other extrinsic impurities with a similar charge-to-mass ratio can be applied as an additional control tool. These include argon ($Z = 18, A = 40$; ionization energy of the fully stripped ions $E_{\text{ioniz.}} \approx 4.4$ keV) and ²²Ne ($Z = 10, A = 22$; $E_{\text{ioniz.}} \approx 1.4$ keV), currently considered for impurity seeding in ITER and future reactors.⁷⁰ Accounting for such impurities, the equivalent concentration of ⁹Be is given by

$$X[^9\text{Be}]_{\text{equiv.}} = X[^9\text{Be}] + (10/4)X[^{22}\text{Ne}] + (18/4)X[\text{Ar}]. \quad (13)$$

The numerical coefficients in Eq. (13) reflect the fact that ²²Ne and Ar ions have a higher charge number than ⁹Be. For example, if the intrinsic level of ⁹Be impurities is about 0.5%, then an additional impurity seeding with $\sim 0.1\% - 0.4\%$ of argon would result in maximizing the RF power absorption on ⁴He ions at concentrations $n(^4\text{He})/n_e \leq 0.5\%$.

VI. SUMMARY AND CONCLUSIONS

ICRF heating of multi-ion species plasmas has been often employed in fusion research. Already in the 1980s, there were theoretical and experimental efforts on the T-10 and TFR tokamaks to use extrinsic impurities such as ²²Ne and Ar to improve the efficiency of ICRF heating and exploit the advantages of the enhanced E_+ RF electric field at the IIH layer in mixed H-D plasmas.⁸⁰⁻⁸² However in those times, second harmonic ICRF heating of impurity ions, $\omega \approx 2\omega_{\text{ci}}$ ($n=2$) was selected as a damping mechanism, which is a finite-Larmor-radius effect.

In multi-ion species plasmas, ICRF heating could be made much more effective using fundamental ($n=1$) heating for a “third” ion population. Sporadic observations of RF power deposition on ions were reported in mixed D-T and D-³He plasmas under conditions where mode conversion was expected. For example, dominant RF power absorption on ⁷Li impurities was reported in D-T experiments on TFTR, designed for electron heating via mode conversion.²¹ Similarly, in ICRF mode conversion experiments in D-³He plasmas, additionally heated with D-NBI, an unexpected generation of high-energy D ions was observed at large $n(^3\text{He})/n_e \approx 25\%$.¹²

The developed theoretical framework for three-ion ICRF scenarios provides a simple and unified explanation for the direct RF absorption by the ions in these experiments, while mode conversion heating was expected. In retrospect, the idea behind these scenarios sounds self-evident. The essential RF physics mechanisms, in particular, the importance of the plasma composition and the presence of impurities in multi-ion species plasmas, the enhanced left-hand RF polarization at the IIH layer, Doppler-shift effects for fast ions, etc., were individually well known by the ICRF community for years and recognized in past ICRF experiments on TFTR, JET, and AUG.

The intentional use of three-ion ICRF scenarios only started a few years ago. Recent experimental and modeling developments of these scenarios on Alcator C-Mod, AUG, and JET tokamaks provided new insights for the exploration of these novel ICRF scenarios for many fields of fusion research, extending their applications beyond the originally intended fast-ion generation and plasma heating.

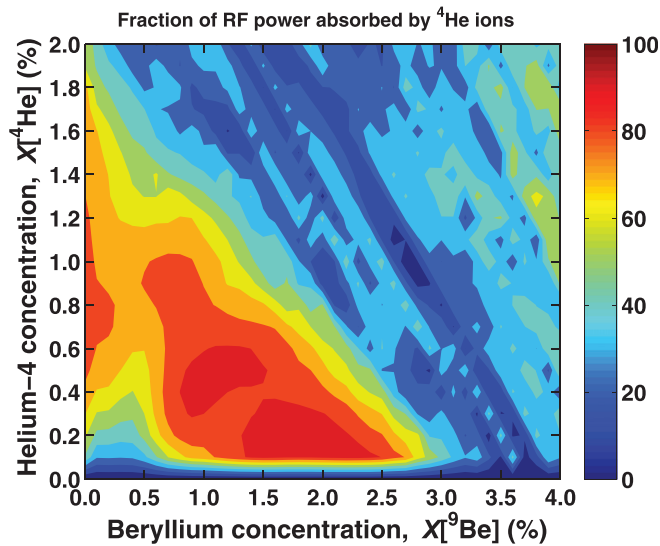


FIG. 20. The fraction of ICRF power absorbed by resonant ⁴He ions in hydrogen majority plasmas, including ⁹Be impurities. The computations were made for the ITER-like plasma conditions using the TORIC code ($B_0 = 5.3$ T, $f = 40$ MHz, $n_{\text{tor}} = 27$, $n_{e0} = 6 \times 10^{19} \text{ m}^{-3}$, and $T_0 = 10$ keV). An additional seeding of ²²Ne and Ar impurities can be applied to complement intrinsic levels of ⁹Be to optimize the three-ion ICRF scenario for ⁴He resonant ions.

As presented in Sec. V, three-ion ICRF scenarios hold promises for ITER to extend the H-mode operational space in its nonactive phase and to provide bulk ion heating of D–T plasmas using intrinsic ^9Be impurities (or in combination with impurities like Ar and ^{22}Ne , considered for impurity seeding). Furthermore, recent experimental results have shown further applications of these scenarios, including many also of relevance for ITER. These include a tool to study fast-ion driven MHD modes, turbulence studies at ITER-relevant fast-ion electron heating conditions, efficient generation of large populations of passing fast ions, local fast-ion current drive and modification of the q -profile, etc.

Three-ion scenarios open new possibilities for the application of ICRF in fusion research, and they also allow revisiting old and sometimes forgotten ideas. As an example, the well-known absorption of ICRF power by alpha particles in D–T plasmas, up until now considered as detrimental, in fact, now opens new potential applications for ICRF in high-temperature fusion-grade plasmas. There is an important and promising field in plasma physics to be further explored.

ACKNOWLEDGMENTS

The authors are grateful to the anonymous reviewers for their constructive comments that allowed us to improve the paper, I. Voitkhovitch for her valuable comments and suggestions during the paper preparation, and to H. Meyer and J. Faustin for fruitful discussions. We thank the ITPA Energetic Particle Physics Topical Group for its support. This work has been carried out within the framework of the EUROfusion Consortium and has received funding from the Euratom research and training programme 2014–2018 and 2019–2020 under Grant Agreement No. 633053. The views and opinions expressed herein do not necessarily reflect those of the European Commission. Part of this work was also carried out in the framework of projects done for the ITER Scientist Fellow Network (ISFN).

ITER is the Nuclear Facility INB No. 174. The views and opinions expressed herein do not necessarily reflect those of the ITER Organization. This publication is provided for scientific purposes only. Its contents should not be considered as commitments from the ITER Organization as a nuclear operator in the frame of the licensing process.

DATA AVAILABILITY

The data that support the findings of this study are available from the corresponding author upon reasonable request.

REFERENCES

- ¹ITER Physics Basis Expert Group on Energetic Particles, Heating and Current Drive and ITER Physics Basis Editors, *Nucl. Fusion* **39**, 2495 (1999).
- ²C. Gormezano, A. C. C. Sips, T. C. Luce, S. Ide, A. Becoulet, X. Litaudon, A. Isayama, J. Hobirk, M. R. Wade, T. Oikawa *et al.*, *Nucl. Fusion* **47**, S285 (2007).
- ³P. U. Lamalle, B. Beaumont, F. Kazarian, T. Gassmann, G. Agarici, T. Alonzo Montemayor, R. Bamber, D. Boilson, A. Cadinot *et al.*, *AIP Conf. Proc.* **1689**, 030007 (2015).
- ⁴B. Beaumont, R. Agarwal, T. Alonzo Montemayor, R. Anand, P. Ajesh, F. Calarco, H. Dalicha, C. Deibele, N. Ferrigno, T. Gassmann *et al.*, *EPJ Web Conf.* **157**, 02002 (2017).
- ⁵J. R. Wilson and P. T. Bonoli, *Phys. Plasmas* **22**, 021801 (2015).
- ⁶J. Ongena, A. Messiaen, Y. O. Kazakov, R. Koch, R. Ragona, V. Bobkov, K. Cromb , F. Durodi , M. Goniche, A. Krivska *et al.*, *Plasma Phys. Controlled Fusion* **59**, 054002 (2017).
- ⁷A. V. Longinov and K. N. Stepanov, in *High-Frequency Plasma Heating*, edited by A. G. Litvak (AIP, New York, 1992), pp. 93–238.
- ⁸J. Adam, *Plasma Phys. Controlled Fusion* **29**, 443 (1987).
- ⁹M. Porkolab, *AIP Conf. Proc.* **314**, 99 (1994).
- ¹⁰J.-M. Noterdaeme, L.-G. Eriksson, M. Mantsinen, M.-L. Mayoral, D. Van Eester, J. Mailloux, C. Gormezano, and T. T. Jones, *Fusion Sci. Technol.* **53**, 1103 (2008).
- ¹¹E. Nelson-Melby, M. Porkolab, P. T. Bonoli, Y. Lin, A. Mazurenko, and S. J. Wukitch, *Phys. Rev. Lett.* **90**, 155004 (2003).
- ¹²M. J. Mantsinen, M.-L. Mayoral, D. Van Eester, B. Alper, R. Barnsley, P. Beaumont, J. Bucalossi, I. Coffey, S. Conroy, M. de Baar *et al.*, *Nucl. Fusion* **44**, 33 (2004).
- ¹³T. H. Stix, *Nucl. Fusion* **15**, 737 (1975).
- ¹⁴J. Wesson, *Tokamaks* (Clarendon, Oxford, 2004).
- ¹⁵M.-L. Mayoral, P. U. Lamalle, D. Van Eester, E. A. Lerche, P. Beaumont, E. De La Luna, P. De Vries, C. Gowers, R. Felton, J. Harling *et al.*, *Nucl. Fusion* **46**, S550 (2006).
- ¹⁶Y. Lin, J. E. Rice, S. J. Wukitch, M. J. Greenwald, A. E. Hubbard, A. Ince-Cushman, L. Lin, M. Porkolab, M. L. Reinke, and N. Tsujii, *Phys. Rev. Lett.* **101**, 235002 (2008).
- ¹⁷Y. O. Kazakov, D. Van Eester, R. Dumont, and J. Ongena, *Nucl. Fusion* **55**, 032001 (2015).
- ¹⁸Y. O. Kazakov, J. Ongena, J. C. Wright, S. J. Wukitch, E. Lerche, M. J. Mantsinen, D. Van Eester, T. Craciunescu, V. G. Kiptily, Y. Lin *et al.*, *Nat. Phys.* **13**, 973 (2017).
- ¹⁹J. Ongena, Y. O. Kazakov, Y. Baranov, C. Hellesen, J. Eriksson, T. Johnson, V. G. Kiptily, M. J. Mantsinen, M. Nocente, R. Bilato *et al.*, *EPJ Web Conf.* **157**, 02006 (2017).
- ²⁰Y. O. Kazakov, M. Nocente, M. J. Mantsinen, J. Ongena, Y. Baranov, T. Craciunescu, M. Dreval, R. Dumont, J. Eriksson, J. Garcia *et al.*, *Nucl. Fusion* **60**, 112013 (2020).
- ²¹J. R. Wilson, R. E. Bell, S. Bernabei, K. Hill, J. C. Hosea, B. LeBlanc, R. Majeski, R. Nazikian, M. Ono, C. K. Philipps *et al.*, *Phys. Plasmas* **5**, 1721 (1998).
- ²²D. V. Reames, *Space Sci. Rev.* **90**, 413 (1999).
- ²³R. Bucik, *Space Sci. Rev.* **216**, 24 (2020).
- ²⁴S. J. Buchsbaum, *Phys. Fluids* **3**, 418 (1960); For completeness, we note that the IIF resonance in this original paper was defined by the condition $\epsilon_S = 0$, corresponding to the resonance of the cold plasma slow wave. However, in the RF literature the notation “IIF resonance” has been historically also used for the fast wave resonance condition $\epsilon_S = n_{\parallel}^2$, a convention we follow in our paper.
- ²⁵M. Brambilla, *Kinetic Theory of Plasma Waves* (Clarendon, Oxford, 1998).
- ²⁶Y. O. Kazakov, D. Van Eester, R. Dumont, J. Ongena, E. Lerche, and A. Messiaen, *AIP Conf. Proc.* **1689**, 030008 (2015).
- ²⁷F. Porcelli, D. Boucher, and M. N. Rosenbluth, *Plasma Phys. Controlled Fusion* **38**, 2163 (1996).
- ²⁸D. Van Eester, E. Lerche, Y. Andrew, T. M. Biewer, A. Casati, K. Cromb , E. de la Luna, G. Ericsson, R. Felton, L. Giacomelli *et al.*, *Plasma Phys. Controlled Fusion* **51**, 044007 (2009).
- ²⁹M. Nocente, A. Dal Molin, N. Eidietis, L. Giacomelli, G. Gorini, Y. Kazakov, E. Khilkevitch, V. Kiptily, M. Iliasova, A. Lvovskiy *et al.*, *Plasma Phys. Controlled Fusion* **62**, 014015 (2020).
- ³⁰P. Sandquist, S. E. Sharapov, M. Lisaka, and T. Johnson, *Phys. Plasmas* **14**, 122506 (2007).
- ³¹Y. O. Kazakov, J. Ongena, R. Bilato, V. Bobkov, J. M. Faustin, A. Kappatou, V. G. Kiptily, E. Lerche, M. Mantsinen, M. Nocente *et al.*, “Recent advances in ICRF heating of mixture plasmas: Survey of JET and AUG experiments and extrapolation to JET-DT and ITER,” in 2018 IAEA Fusion Energy Conference, Gandhinagar (EX/8-1) (2018); available at <https://conferences.iaea.org/indico/event/151/papers/5659/files/4827-Kazakov-IAEA-FEC2018-paper-v5.pdf>.
- ³²V. Kiptily, Y. Kazakov, M. Fitzgerald, M. Nocente, M. Iliasova, E. Khilkevitch, M. Mantsinen, M. F. F. Nave, J. Ongena, S. E. Sharapov *et al.*, *Nucl. Fusion* **60**, 112003 (2020).
- ³³L.-G. Eriksson, T. Hellsten, and U. Will n, *Nucl. Fusion* **33**, 1037 (1993).
- ³⁴R. J. Hawryluk, “An empirical approach to tokamak transport,” in *Physics of Plasmas Close to Thermonuclear Conditions*, edited by B. Coppi *et al.* (CEC, Brussels, 1981), Vol. 1, pp. 19–46.

- ³⁵M. Brambilla, *Plasma Phys. Controlled Fusion* **41**(1), 1 (1999).
- ³⁶M. J. Mantsinen, V. Bobkov, D. Gallart, A. Kappatou, Y. O. Kazakov, and M. Weiland, in Proceedings of 46th European Physical Society Conference on Plasma Physics (EPS), Milan, Italy (2019), p. O5.102, <http://ocs.ciemat.es/EPS2019ABS/pdf/O5.102.pdf>.
- ³⁷K. K. Kirov, Y. Kazakov, M. Nocente, J. Ongena, Y. Baranov, F. Casson, J. Eriksson, L. Giacomelli, C. Hellesen, V. Kiptily *et al.*, *AIP Conf. Proc.* **2254**, 030011 (2020).
- ³⁸ITER Organization, "ITER research plan within the staged approach," ITER Technical Report No. ITR-18-003 (2018); available at <https://www.iter.org/technical-reports>.
- ³⁹M. Nocente, Y. O. Kazakov, J. Garcia, V. G. Kiptily, J. Ongena, M. Dreval, M. Fitzgerald, S. E. Sharapov, Z. Stancar, H. Weisen *et al.*, *Nucl. Fusion* **60**, 124006 (2020).
- ⁴⁰S. E. Sharapov, T. Hellsten, V. G. Kiptily, T. Craciunescu, J. Eriksson, M. Fitzgerald, J.-B. Girardo, V. Goloborod'ko, C. Hellesen, A. Hjalmarsson *et al.*, *Nucl. Fusion* **56**, 112021 (2016).
- ⁴¹S. Mazzi, J. Garcia, D. Zarzoso, Y. O. Kazakov, J. Ongena, M. Nocente, M. Dreval, Z. Stancar, G. Szepesi, J. Eriksson *et al.*, "Towards enhanced performance in fusion plasmas via turbulence suppression by MeV ions" (to be published); [arXiv:2010.07977](https://arxiv.org/abs/2010.07977).
- ⁴²F. Jenko, W. Dorland, M. Kotschenreuther, and B. N. Rogers, *Phys. Plasmas* **7**, 1904 (2000).
- ⁴³B. N. Breizman, H. L. Berk, and M. S. Pekker, *Phys. Plasmas* **10**, 3649 (2003).
- ⁴⁴A. N. Kaufman, *Phys. Fluids* **15**, 1063 (1972).
- ⁴⁵L.-G. Eriksson, M. J. Mantsinen, T. Hellsten, and J. Carlsson, *Phys. Plasmas* **6**, 513 (1999).
- ⁴⁶T. Hellsten, T. Johnson, J. Carlsson, L.-G. Eriksson, J. Hedin, M. Laxåback, and M. Mantsinen, *Nucl. Fusion* **44**, 892 (2004).
- ⁴⁷L.-G. Eriksson, A. Mueck, O. Sauter, S. Coda, M. J. Mantsinen, M.-L. Mayoral, E. Westerhof, R. J. Buttery, D. McDonald, T. Johnson *et al.*, *Phys. Rev. Lett.* **92**, 235004 (2004).
- ⁴⁸B. Bigot, *Nucl. Fusion* **59**, 112001 (2019).
- ⁴⁹E. Lerche, D. Van Eester, J. Ongena, M.-L. Mayoral, T. Johnson, T. Hellsten, R. Bilato, A. Czarnecka, R. Dumont, C. Giroud *et al.*, *AIP Conf. Proc.* **1406**, 245 (2011).
- ⁵⁰E. Lerche, D. Van Eester, T. J. Johnson, T. Hellsten, J. Ongena, M.-L. Mayoral, D. Frigione, C. Sozzi, G. Calabro, M. Lennholm *et al.*, *Plasma Phys. Controlled Fusion* **54**, 074008 (2012).
- ⁵¹M. Schneider, J.-F. Artaud, P. Bonoli, Y. Kazakov, P. Lamalle, E. Lerche, D. Van Eester, and J. Wright, *EPJ Web Conf.* **157**, 03046 (2017).
- ⁵²V. Bobkov, F. Braun, R. Dux, A. Herrmann, H. Faugel, H. Fünfgelder, A. Kallenbach, R. Neu, J.-M. Noterdaeme, R. Ochoukov *et al.*, *Nucl. Fusion* **56**, 084001 (2016).
- ⁵³V. Bobkov, D. Aguiam, R. Bilato, S. Brezinsek, L. Colas, H. Faugel, H. Fünfgelder, A. Herrmann, J. Jacquot, A. Kallenbach *et al.*, *Plasma Phys. Controlled Fusion* **59**, 014022 (2017).
- ⁵⁴H. Meyer, for AUG Team: D. Aguiam, C. Angioni, C. G. Albert, N. Arden, R. Arredondo Parra, O. Asunta, M. de Baar, M. Balden, V. Bandaru *et al.*, *Nucl. Fusion* **59**, 112014 (2019).
- ⁵⁵U. Plank, T. Pütterich, C. Angioni, M. Cavedon, G. D. Conway, R. Fischer, T. Happel, A. Kappatou, R. M. McDermott, P. A. Schneider *et al.*, *Nucl. Fusion* **60**, 074001 (2020).
- ⁵⁶R. Bilato, M. Brambilla, O. Maj, L. D. Horton, C. F. Maggia, and J. Stober, *Nucl. Fusion* **51**, 103034 (2011).
- ⁵⁷A. Kappatou, M. Weiland, R. Bilato, Y. O. Kazakov, R. Dux, V. Bobkov, B. Geiger, T. Pütterich, and R. M. McDermott, in Proceedings of 45th EPS Conference on Plasma Physics (2018), p. O2.105; available at <http://ocs.ciemat.es/EPS2018PAP/pdf/O2.105.pdf>.
- ⁵⁸A. Kappatou, M. Weiland, R. Bilato, Y. O. Kazakov, R. Dux, V. Bobkov, T. Pütterich, and R. M. McDermott, "CXRS measurements of energetic helium ions in ASDEX Upgrade plasmas heated with a three-ion ICRF scenario," *Nucl. Fusion* **61**, 036017 (2021).
- ⁵⁹Y. O. Kazakov, J. Ongena, D. Van Eester, R. Bilato, R. Dumont, E. Lerche, M. Mantsinen, and A. Messiaen, *Phys. Plasmas* **22**, 082511 (2015).
- ⁶⁰E. Lerche, D. Van Eester, P. Jacquet, F. Casson, Y. Baranov, P. Dumortier, D. Gallart, P. Huynh, T. Johnson, Y. Kazakov *et al.*, *AIP Conf. Proc.* **2254**, 030007 (2020).
- ⁶¹D. F. H. Start, J. Jacquinot, V. Bergeaud, V. P. Bhatnagar, S. W. Conroy, G. A. Cottrell, S. Clement, G. Ericsson, L.-G. Eriksson, A. Fasoli *et al.*, *Nucl. Fusion* **39**, 321 (1999).
- ⁶²D. S. Darrow, R. Majeski, N. J. Fisch, R. F. Heeter, H. W. Herrmann, M. C. Herrmann, M. C. Zarnstorff, and S. J. Zweben, *Nucl. Fusion* **36**, 509 (1996).
- ⁶³J.-M. Noterdaeme, M. Brambilla, B. Brüsehaber, R. Dux, H.-U. Fahrbach, W. Becker, F. Braun, H. Faugel, D. Hartmann, F. Hofmeister, and F. Wesner, in Proceedings of the 26th EPS Conference on Plasma Physics (1999), p. 1561; available at <http://epsppd.epfl.ch/Maas/web/pdf/p4050.pdf>.
- ⁶⁴P. U. Lamalle, M. J. Mantsinen, J.-M. Noterdaeme, B. Alper, P. Beaumont, L. Bertalot, T. Blackman, V. V. Bobkov, G. Bonheure, J. Brzozowski *et al.*, *Nucl. Fusion* **46**, 391 (2006).
- ⁶⁵D. Van Eester, E. Lerche, T. J. Johnson, T. Hellsten, J. Ongena, M.-L. Mayoral, D. Frigione, C. Sozzi, G. Calabro, M. Lennholm *et al.*, *Plasma Phys. Controlled Fusion* **54**, 074009 (2012).
- ⁶⁶J. Garcia, T. Görler, and F. Jenko, *Phys. Plasmas* **25**, 055902 (2018).
- ⁶⁷M. Salewski, M. Nocente, B. Madsen, I. Abramovic, M. Fitzgerald, G. Gorini, P. C. Hansen, W. W. Heidbrink, A. S. Jacobsen, T. Jensen *et al.*, *Nucl. Fusion* **58**, 096019 (2018).
- ⁶⁸M. Garcia-Munoz, S. E. Sharapov, M. A. Van Zeeland, E. Ascasibar, A. Cappa, L. Chen, J. Ferreira, J. Galdon-Quiroga, B. Geiger, J. Gonzalez-Martin *et al.*, *Plasma Phys. Controlled Fusion* **61**, 054007 (2019).
- ⁶⁹A. Di Siena, T. Görler, E. Poli, A. Banon Navarro, A. Biancalani, R. Bilato, M. J. Mantsinen, F. N. deOliveira-Lopes, and F. Jenko, *Nucl. Fusion* **59**, 124001 (2019).
- ⁷⁰A. Kallenbach, M. Bernert, R. Dux, L. Casali, T. Eich, L. Giannone, A. Herrmann, R. McDermott, A. Mlynek, H. W. Müller *et al.*, *Plasma Phys. Controlled Fusion* **55**, 124041 (2013).
- ⁷¹M. Maslov, J. Citrin, P. Jacquet, Y. Kazakov, D. L. Keeling, D. B. King, E. Lerche, M. Marin, J. Ongena, and D. Van Eester, in Proceedings of 46th EPS Conference on Plasma Physics (2019), p. O5.104; available at <http://ocs.ciemat.es/EPS2019PAP/pdf/O5.104.pdf>.
- ⁷²D. Van Eester, F. Louche, and R. Koch, *Nucl. Fusion* **42**, 310 (2002).
- ⁷³Y. O. Kazakov, V. G. Kiptily, S. E. Sharapov, and D. Van Eester, *Nucl. Fusion* **52**, 094012 (2012).
- ⁷⁴H. Weisen, A. C. C. Sips, C. D. Challis, L.-G. Eriksson, S. E. Sharapov, P. Batistoni, L. D. Horton, K.-D. Zastrow, and EFDA-JET Contributors, *AIP Conf. Proc.* **1612**, 77 (2014).
- ⁷⁵E. Joffrin, S. Abduallev, M. Abhangi, P. Abreu, V. Afanasev, M. Afzal, K. M. Aggarwal, T. Ahlgren, L. Aho-Mantila, N. Aiba *et al.*, *Nucl. Fusion* **59**, 112021 (2019).
- ⁷⁶R. Dumont, J. Mailloux, V. Aslanyan, M. Baruzzo, C. D. Challis, I. Coffey, A. Czarnecka, E. Delabie, J. Eriksson, J. Faustin *et al.*, *Nucl. Fusion* **58**, 082005 (2018).
- ⁷⁷L.-G. Eriksson and T. Hellsten, *Nucl. Fusion* **29**, 875 (1989).
- ⁷⁸J. C. Hillesheim, E. Delabie, E. R. Solano, I. S. Carvalho, A. Drenik, C. Giroud, A. Huber, E. Lerche, B. Lomanowski, M. Mantsinen *et al.*, in Proceedings of 44th EPS Conference on Plasma Physics (2017), p. P5.162; available at <http://ocs.ciemat.es/EPS2017PAP/pdf/P5.162.pdf>.
- ⁷⁹Y. O. Kazakov, M. Schneider, J. Ongena, R. Bilato, R. Dumont, J. M. Faustin, E. Lerche, D. Van Eester, and J. C. Wright, in Proceedings of 45th EPS Conference on Plasma Physics (2018), p. P5.1047; available at <http://ocs.ciemat.es/EPS2018PAP/pdf/P5.1047.pdf>.
- ⁸⁰A. V. Longinov, S. S. Pavlov, and K. N. Stepanov, "The use of heavy admixture ions for enhancing the ICRF plasma heating efficiency," in Proceedings of 12th European Conference on Controlled Fusion and Plasma Physics, Budapest, Hungary (1985), Vol. 2, pp. 132–135.
- ⁸¹V. V. Alikae, E. L. Berezovskij, N. A. Vasin, V. L. Vdovin, A. N. Vertiporokh, S. L. Efmov, V. S. Zaveryaev, Y. S. Maksimov, G. E. Notkin, A. V. Chesnokov, N. V. Shapotkovskij, E. D. Kramskoj, A. V. Longinov, G. A. Miroshnichenko, S. S. Pavlov, K. N. Stepanov, V. A. Tsurikov, and A. A. Chmyga, "ICRH experiments in T-10 tokamak," in Proceedings of 12th European Conference on Controlled Fusion and Plasma Physics, Budapest, Hungary (1985), Vol. 2, pp. 156–159.
- ⁸²TFR Group, M. H. Achard, J. Adam, E. Anabitarte, J. Andreoletti, P. Babelier, H. Barkley, C. Breton, J. Breton, R. Brugnetti, H. Capes *et al.*, *Nucl. Fusion* **26**, 873 (1986).